Thesis for the Master's degree in Molecular Biosciences
Main field of study in Biochemistry
60 study points

Studies of Electron Transfer from Flavodoxin Reductase to NrdI in *Bacillus cereus*

by Silje Skråmo

Department of Molecular Biosciences
Faculty of Mathematics and Natural Biosciences
UNIVERSITY OF OSLO 06/2012

Acknowledgements

The work presented in this thesis has been carried out in the laboratory of Professor K. Kristoffer Andersson at the Department of Molecular Biosciences, University of Oslo.

First, I want to thank Professor K. Kristoffer Andersson for letting me do a master project in his group, and for introducing me to the interesting field of metalloproteins that they are working in. I am also very thankful for the conferences, meetings and synchrotron trips he has sent me to. In addition to him, have my co-supervisors Hans-Petter Hersleth, Marta Hammerstad and Åsmund K. Røhr given me excellent supervision during the whole period that I have been working on my master project, and we have had interesting talks and discussions that have taught me a lot. I want to thank them for that, and for always being there.

I will also thank Marie, Mari, my other fellow students and the group for the great social environment they make; for the lunch breaks, the laughter, the dinners, the trips, and for always making me smile.

Finally, I want to thank Bjørn, mamma, pappa and Kim for all the support, love and understanding.

Oslo, June 2012
Silje Skråmo

Abstract

Ribonucleotide reductase (RNR) catalyses the reduction of the four ribonucleotides to their corresponding deoxyribonucleotides needed for synthesis and repair of DNA. RNR is found in the genome of all living organisms, indicating that this enzyme is an essential part of the fundamentals of life. The RNRs explored to date are divided into three different main classes; Ia-c, II and III.

The cofactor of class Ib RNRs was recently shown to be a dimanganese cluster. Further that the flavoprotein NrdI is essential for the generation of the dimanganese-tyrosyl radical, the active form of the cofactor. An active cofactor is, in turn, essential for generation of a protein radical in the catalytic site, which initiates substrate turnover. The function of NrdI in class Ib RNR is, however, not fully understood. Two flavodoxin reductases (FldRs) have been located in the genome of *Bacillus cereus (B. cereus),* and considered as potential reducers of NrdI by transferring electrons from NADPH to NrdI. Investigations in their ability to interact with and reduce NrdI, would enhance the knowledge about the function of NrdI.

This master project has focused on the two FldRs found in *B. cereus*. One of them was cloned, and both were expressed and purified. One of the FldRs is expressed primary as apo protein, and work was performed to reconstitute cofactor-containing protein from apo-FldR and flavin. Initial protein crystals were obtained for both proteins, but no complete datasets could be collected. The ability of each FldR to reduce NrdI and two other flavodoxins from *B. cereus* was tested. The result suggests that the redox partners of both FldRs are other than NrdI. Initial kinetic measurements were performed with 2,6-dichlorophenolindophenol (DCPIP) as the electron acceptor, resulting in a 200-fold difference in the Km values of the respective FldRs. Their ability to reduce cytochrome *c* (Cyt*c*) was also tested. In sum, the experiments with the two-electron acceptor DCPIP and the one-electron acceptor Cyt*c* indicated that one FldR is the most effective two-electron donor, and the other FldR is the most effective one-electron donor.

Table of contents

Abbreviations

B. cereus	*Bacillus cereus*
BL21-cells	*E. coli* BL21 (DE3) Competent cells
Cyt*c*	cytochrome *c*
DCPIP	2,6-dichlorophenolindophenol
E. coli	*Escherichia coli*
Fld	flavodoxin
FldR	Flavodoxin reductase
FMN	flavin mononucleotide
hq	hydroquinone
LB	Luria Broth
NADH	nicotinamide adenine dinucleotide
NADPH	nicotinamide adenine dinucleotide
ox	oxidised
PCR	polymerase chain reaction
PX	protein X-ray crystallography
redox	reduction-oxidation
RNR	Ribonucleotide reductase
SDS-PAGE	sodium dodecyl sulphate polyacrylamide gel electrophoresis
sq	semiquinone
TB	Terrific Broth
UV-vis	Ultraviolet and visible light
V_0	initial velocity
XL10-cells	*E. coli* XL10-Gold ultracompentent cells

1. Introduction

1.1. Ribonucleotide reductase

1.1.1. Many different ribonucleotide reductases

Deoxyribonucleotides, the precursors of DNA, are generated by the reduction of ribonucleotides, the precursors of RNA. The reduction is a radical-induced process, and takes place by the 2′-hydroxyl group on the ribose ring being replaced by a hydrogen atom (**Figure 1.1**).

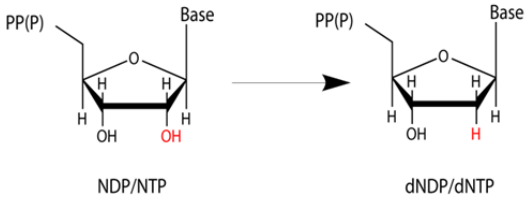

Figure 1.1: Ribonucleotide di- and triphosphates are converted to deoxyribonucleotide di- and triphosphates by reduction of the 2'-hydroxyl group in the ribose ring.

The enzyme ribonucleotide reductase (RNR) catalyses this reaction for all four DNA precursors, and appear to do so in all living species which so far have been sequenced, as well as in some virus. Hence, it is assumed that all organisms depend on this machinery for de novo production of deoxyribonucleotides. All known RNRs share a common reaction mechanism and contain two distinct functional components; a ribonucleotide binding site and a radical generator (cofactor). Despite little sequence similarity, detailed studies have revealed that several crucial residues are conserved among the RNRs of different organisms, many of which are located in the substrate binding site. Additionally, the three-dimensional structural features of the RNRs studied to date, indicate that the substrate binding sites of these enzymes are structurally homologues [Berg, Tymoczko and Stryer, 2007; Eklund et al., 2001; Jordan and Reichard, 1998; Nordlund and Reichard, 2006; Tomter et al., 2012].

The first RNR to be discovered some 50 years ago was from *Escherichia coli* (*E. coli*) [Reichard, Baldesten and Rutberg, 1961]. Soon after the discovery of the same enzyme in *Lactobacillus leichmannii* [Blakley and Barker, 1964], it became clear that RNR can catalyse ribonucleotide reduction by the use of different cofactors. Since then, several other RNRs

with varying cofactors have been discovered, and are today divided into three main classes, namely Ia-c, II and III [Cotruvo and Stubbe, 2011b] (**Figure 1.2**). Several organisms encode RNRs from different classes – some even from all three classes – and the expression of the different RNRs depend on the environmental conditions. With the exception of *Euglena gracilis* [Hamilton, 1973], class Ia RNRs are found in all eukaryotes from yeast to human and in prokaryotes, viruses and bacteriophages. Class Ia RNRs depend on oxygen for functionality, hence active enzymes from this class are not found in strict anaerobes. Class Ib RNRs are found in a wide range of facultative and obligate aerobic prokaryotes. Class Ic was discovered more recently in *Chlamydia trachomatis* [Roshick, Iliffe-Lee and McClarty, 2000], and determination of its sequence suggests its presence in the genomes of some archaea and eubacteria, with some of the eubacteria being thermophiles [Högbom et al., 2004]. Class II RNRs are microbial enzymes that occur in both aerobic and anaerobic organisms. Class III RNRs depend on anaerobic environments to function, and are found in both strict anaerobic and facultative anaerobic organisms (i.e. organisms that performs aerobic respiration when O_2 is present and fermentation when it is absent) and a few unicellular eukaryotes [Cotruvo and Stubbe, 2011b; Jiang et al., 2007; Nordlund and Reichard, 2006; Reichard, 1993].

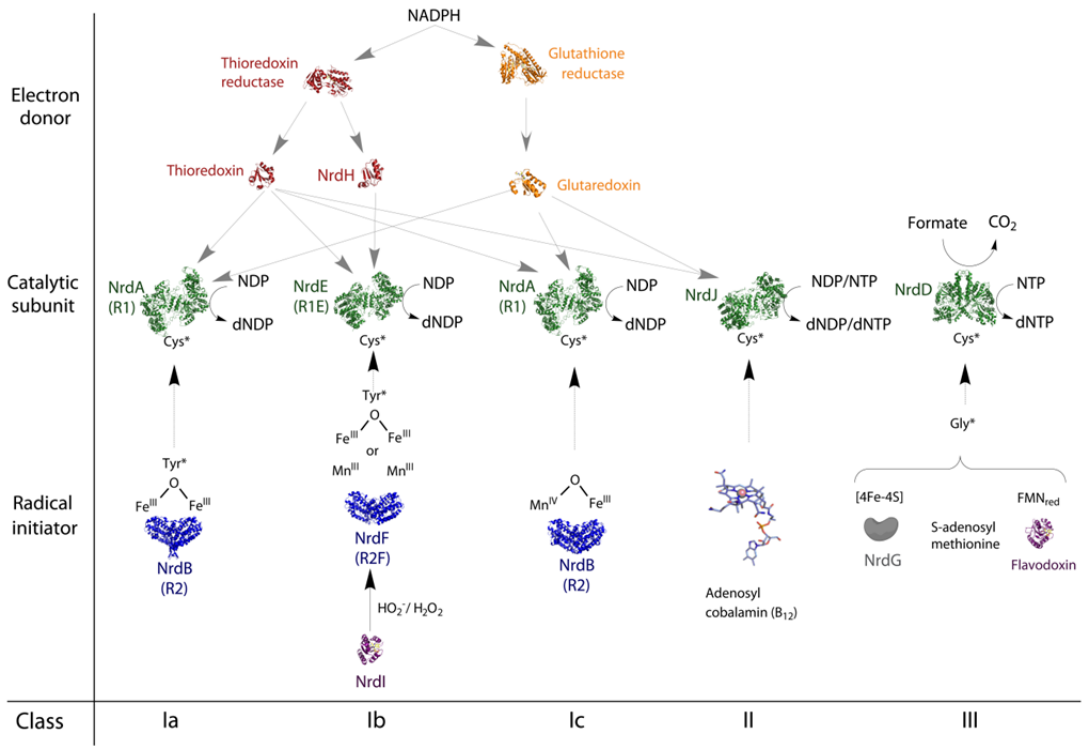

Figure 1.2: Overview of the different classes of RNR. Adapted from Tomter et al., 2012.

All three classes are proposed to use a thiyl radical (S•) for the initiation of substrate turnover, and the generation of the S• is accomplished via oxidative power derived from the different cofactors (**Figure 1.2**). Class Ia RNRs utilises a diiron tyrosyl radical ($Fe^{III}Fe^{III}$-Y•) as the cofactor [Sjöberg, et al., 1977], class Ib is more recently been proposed to utilise a dimanganese tyrosyl radical ($Mn^{III}Mn^{III}$-Y•) [Cox et al., 2010; Jordan et al., 1994] instead of a $Fe^{III}Fe^{III}$-Y•, and for class Ic it is proposed to be a stable diiron ($Fe^{IV}Fe^{III}$) or manganese-iron ($Mn^{IV}Fe^{III}$) cluster (**Figure 1.3**) [Jiang et al., 2007, Voevodskaya et al., 2007].

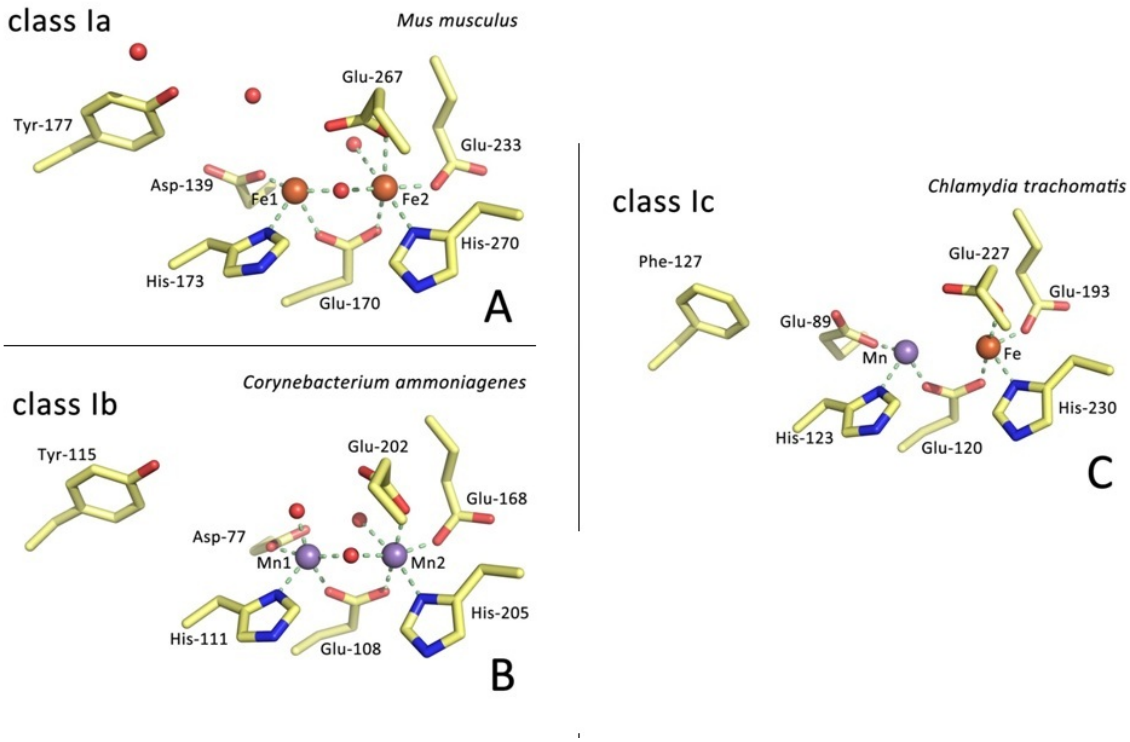

Figure 1.3: Metal cofactor structures found in class Ia, class Ib and class Ic RNR. A) Class Ia RNR from mouse (PDB code 1W68) with both metal centres occupied by iron, B) class Ib RNR from *C. ammoniagenes* (PDB code 3MJO) with both metal centres occupied by manganese and C) class Ic RNR from *C. trachomatis* (coordinates is from Martin Högbom) with one metal centre occupied by iron and the other by manganese. Figure adapted from Tomter et al., 2012.

The RNRs of class I are composed of two types of subunits, designated R1 (α) and R2 (β), where R1 housed the substrate binding site and R2 harbours the metal cofactor (**Figure 1.2**). The quarternary structures of the class I enzymes are actively investigated, but are best understood for the class Ia RNRs from *E. coli* and mouse. In this class, there is a general consensus that the active form is $\alpha_2\beta_2$ (**Figure 1.4**), whereas it is proposed to be more complex in eukaryotes [Fairman et al., 2011; Hofer et al., 2012; Kashlan et al., 2002;

Rofougaran, Vodnala and Hofer, 2006]. Class II RNRs are O_2-independent and use adenosylcobalamin as the S• generator, and class III RNRs use a glycyl radical for this purpose, which is generated by a $(4Fe4S)^{1+/2+}$ cluster together with S-adenosylmethionine. These enzymes have structures similar to the R1 subunits of class I, but they lack analogues to the R2 subunits as the nature of the cofactors to a large extent deviates from those of the class I RNRs [Stubbe and van der Donk, 1998] (**Figure 1.2**).

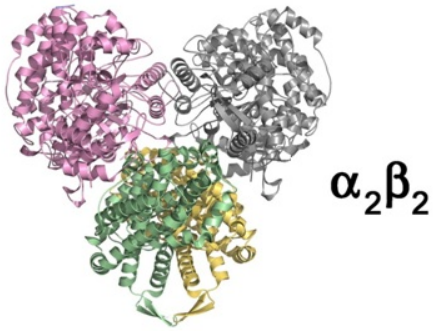

Figure 1.4: The proposed $\alpha_2\beta_2$ model from *E. coli*, where the subunits are docked along their symmetry axis (PDB codes: 3R1R, 1RIB). Adapted from Tomter et al., 2012.

1.1.2. The enzymatic reaction

The enzymatic reaction was first postulated after experiments with isotopic labelled nucleosides in rat [Hammarsten, Reichard and Saluste, 1950]. 26 years later, a tyrosine residue serving as the protein radical was observed in the polypeptide chain of an RNR, supporting the postulation [Reichard and Ehrenberg, 1983]. The S• of the protein generates a substrate radical, which in turn leads to the reduction of the ribonucleotide to a deoxyribonucleotide, through a mechanism which is common for all RNRs. The following description focuses on class I (and II) RNRs, but still describes the general mechanism of class II and III RNR as well. Initially, the cofactor of the R2 subunit is oxidised to a protein radical. The radical is transferred~35 Å to the R1 subunit, where it leads to the oxidation of a conserved cysteine residue in the active site to an S•. The S• then initiates a complex, radical-mediated reduction process by abstracting the nucleotide´s 3′-hydrogen atom, which is returned to the 3′-position at the end of the reaction (**Figure 1.5**). The direct source of electrons required for nucleotide reduction is two conserved cysteines in the active sites of class I and II RNRs. The re-reduction of this electron source is necessary for multiple turns of

nucleotide reduction to take place, and this is accomplished by using electrons from thioredoxin or glutaredoxin (**Figure 1.2**) [Cotruvo and Stubbe, 2011b; Kolberg et al., 2004; Licht, Gerfen and Stubbe, 1996; Mao et al., 1992; Stubbe and van der Donk, 1998]. In class III RNRs, only one of these two cysteines is intact; instead, an asparagine residue is located in an equivalent position. Hence, formation of the disulphide bond, a critical step in the proposed mechanism for class I and II, is clearly not relevant for this class. It has been shown that formate functions as a reductant in class III RNRs (**Figure 1.2**) [Mulliez, et al., 1995], and on the basis of structural studies, it seems likely that the formate binds in the active site, where it would be directly involved in the reduction reactions [Logan et al., 1999].

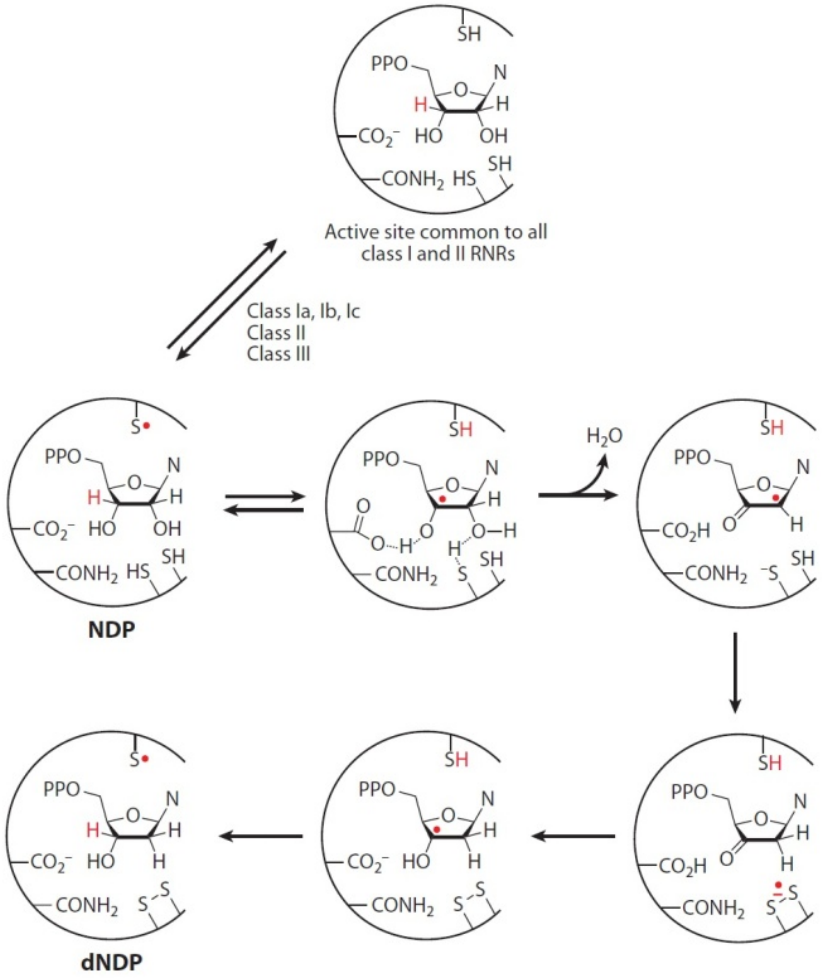

Figure 1.5: The proposed mechanism of ribonucleotide reduction by RNRs. The active sites of all three classes of RNRs share a conserved cysteine on the top face of the substrate. This residue is oxidised to an S• by the radical generating component of the RNR in the first step of catalysis. The S• initiates substrate reduction by abstraction of the nucleotides' 3′ hydrogen atom (red), which is returned to the 3′ position in the product at the end of the reaction [Licht, Gerfen and Stubbe, 1996]. Adapted from Cotruvo and Stubbe, 2011b.

1.2. Class Ib RNR

1.2.1. The identity of the class Ib RNR metal cofactor

The identity of the metal ions in the cofactor required for an active class Ib RNR *in vivo,* has been debated for nearly three decades. However, until more recently it was generally thought that the class Ib RNR contained a $Fe^{III}Fe^{III}$-Y• cofactor in the same way as class Ia RNR. Indications of the existence of a manganese-dependent RNR came from observations in *Corynebacterium* species. During industrial production of amino acids and nucleotides, it was experienced several defects under manganese deficiency, namely unbalanced growth, cell elongation, loss of viability and arrest of DNA synthesis. At the same time, RNA, protein and peptidoglycan synthesis were unaffected. These indications led to a study of *Corynebacterium ammoniagenes* (*C. ammoniagenes*) with regard to the metal ions required for an active RNR [Willing, Follman and Auling, 1978]. The study concluded that manganese ions is most likely required for the formation of an active cofactor rather than iron ions, because the R2-subunit was associated with the radioactive ^{54}Mn from the growth medium [Willing, Follman and Auling, 1978]. The crystal structure of the R2-subunit of RNR from *C. ammoniagenes* was reported many years later, with the observation that the metal site contains an oxo/hydroxo-bridged manganese dimer, located near a tyrosine residue, hence confirming the previous indications [Cox et al., 2010]. Moreover, recent quantification of the metal content in class Ib RNR from another species of this genus, namely *Corynebacterium glutamicum*, revealed 0.06 mol Fe but 0.8 mol Mn per mol R2-monomer, which would assign two manganese atoms bound to the dimeric metal cofactor [Abbouni et al., 2009]. The fact that *E. coli* class Ib RNR is expressed under conditions of iron-limitation and oxidative stress, has also supported the existence of a class I RNR that requires a metal other than iron to obtain an active RNR [Monje-Casas et al., 2001; McHugh et al., 2003]. Although class Ib RNR from *E. coli* have shown to be active with a $Fe^{III}Fe^{III}$-Y• cofactor *in vitro* [Roca et al., 2008], this enzyme is also active *in vitro* in its manganese form, i.e. with a $Mn^{III}Mn^{III}$-Y• cofactor, and self-assembly *in vitro* have been demonstrated [Cotruvo and Stubbe, 2010]. The enzyme has also shown to utilise a $Mn^{III}Mn^{III}$-Y• cofactor *in vivo* under iron-limited conditions [Cotruvo and Stubbe, 2011a], and it has been established that *E. coli* requires manganese under conditions of chronic H_2O_2 stress [Anjem, Varghese and Imlay, 2009]. Oxidative stress is another condition which is reported to increase the level of class Ib RNR expression [Cotruvo and Stubbe, 2011b]. Additionally, in two *Bacillus* species, the $Mn^{III}Mn^{III}$-Y• form has been demonstrated to be more active than the iron forms [Crona et al., 2011].

1.2.2. Generation of an active metal cofactor – the importance of NrdH and NrdI

The operon structures of the genes encoding the class I RNRs are *nrdAB* for subclass Ia, *nrdHIEF* for subclass Ib and *nrdAB*^{Phe} for subclass Ic. In the case of class Ia and Ic RNRs, the NrdA proteins corresponds to the R1 subunits and the NrdB/NrdB^{Phe} proteins corresponds to the R2 subunits (**Figure 1.2**). In the case of class Ib RNRs, the NrdE protein corresponds to the R1 subunit and the NrdF protein corresponds to the R2 subunit. Two additional proteins, NrdH and NrdI, are required for the regulation of class Ib RNRs and is either cotranscribed with the *nrdEF* or often transcribed in a coordinated fashion when the operon structure is different, i.e. when *nrdH* and *nrdI* are located elsewhere in the genome [Jordan, Aragall et al., 1996; Monje-Casas et al., 2001; Torrents, Roca and Gibert, 2003].

NrdH is a 9 kDa protein with a conserved CXXC motif which is characteristic for thiol-disulfide oxidoreductases [Stehr et al., 2001]. Biochemical studies have demonstrated that it can act as an electron donor for NrdE, suggesting it to be the *in vivo* reducer of the two substrate-reducing cysteines in the active site (**Figure 1.5**) [Jordan et al., 1997; Jordan, Pontis et al., 1996]. In fact, NrdH have shown *in vitro* to be responsible for a 10-fold elevation of the activity of the manganese form of *Bacillus anthracis* and *Bacillus cereus* (*B. cereus*) class Ib RNRs compared to that of the iron form of the enzymes [Crona et al., 2011]. *E. coli* contains the genes for both class Ia and Ib RNR, and studies comparing the specificity and physiological roles of NrdH culminates with NrdH being the physiological reducer of NrdE in this organism. NrdH receives electrons from the thioredoxin reductase that also delivers electrons to thioredoxin, which is the physiological reducer of NrdA in *E. coli* [Gon, Faulkner and Beckwith, 2006; Jordan et al., 1997]. NrdH may therefore be specific for class Ib RNR, and considered as an *in vivo* analogue to the thioredoxin or glutaredoxin in class Ia RNR (**Figure 1.2**), with which it has been shown to share considerable similarities [Jordan, Pontis et al., 1996, Stehr et al., 2001]. NrdH is, however, not considered a member of the glutaredoxins because it lacks a specific sequence responsible for glutathione binding [Bushweller et al., 1994]. In addition, the active site sequence C-M/V-Gln-C differs from the typical C-P-Y-C of glutaredoxins and from the conserved C-G-P-C of thioredoxins [Gon, Faulkner and Beckwith, 2006].

NrdI is a 15 kDa protein with a flavin mononucleotide (FMN) cofactor as the redox-active component and a flavodoxin-like fold (**Figure 1.6** and **Figure 1.7**). The protein was isolated and characterised for the first time in 2008 [Roca et al., 2008; Johansson et al., 2010], when it was shown to be essential for the functionality of NrdHEF from *Streptococcus pyogenes* (*S. pyogenes*).

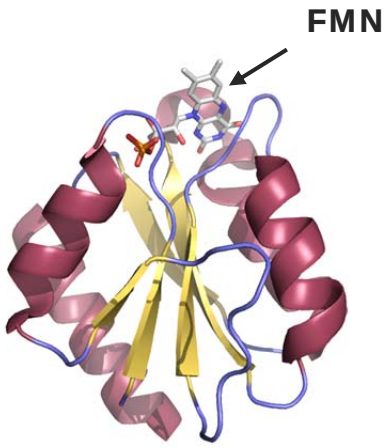

Figure 1.6: NrdI from *B. cereus* with a flavodoxin-like fold, where two α-helical layers sandwitches a 5-stranded parallel β-sheet. The flavin cofactor FMN (gray, on the top of the molecule) is in its oxidised form (PDB code 2X2O). The figure was made using PyMOL (The PyMOL Molecular Graphics System, Version 1.5.0.4 Schrödinger, LLC).

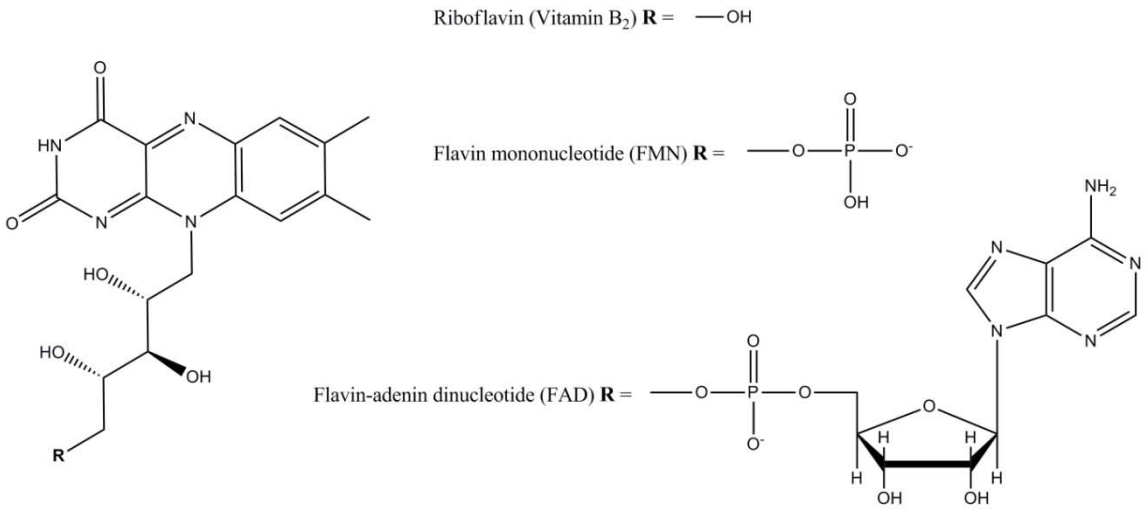

Figure 1.7: Assembly of flavin based cofactors.

During the same year, the FMN cofactor of NrdI from *E. coli* was shown to possess unusual reduction-oxidation (redox) properties compared to those of typical flavodoxins (Flds). Flavin cofactors can have several different redox states; they can be in an oxidised (ox), partially reduced or fully reduced form. The partially reduced form can be anionic or neutral and is called semiquinone (sq). The fully reduced form can be anionic or neutral as well, and the neutral, fully reduced form is called hydroquinone (hq) (**Figure 1.8**).

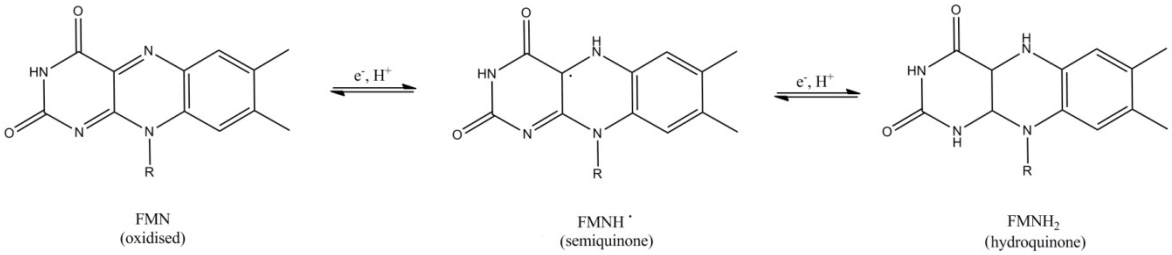

Figure 1.8: Flavin redox states, using FMN as an example. The ox form is yellow, the sq form is blue and the hq form is colourless.

Because of these redox properties, they are capable of switching between one- and two-electron transfer. On binding to a specific protein, the equilibrium between the different redox-states of the flavin can change dramatically. Some enzymes show essentially no stabilisation of sq, while others give almost 100 % stabilisation [Massey, 2000]. The physiological role of typical Flds is to be a one-electron reductant, as the $E_{ox/sq}$ is between -50 and -220 mV and the $E_{sq/hq}$ is between -370 and - 450 mV. This means that the $E_{ox/sq}$ is lowered compared to that of free FMN, whereas the $E_{ox/sq}$ is heightened [Cotruvo and Stubbe, 2008; Draper and Ingrahm, 1968; Hoover et al., 1999]. For NrdI, on the other hand, $E_{ox/sq}$ and $E_{sq/hq}$ are approximately equal, thereby making it a good candidate for a two-electron reducer (**Table 1.1**).

Table 1.1: Reduction potentials of different redox-states of FMN free in solution, FMN bound to flavodoxin and FMN bound to the flavodoxin-like, NrdI, respectively.

	FMN free in solution	**Fld-bound FMN**	**NrdI-bound FMN**
$E_{ox/sq}$ **(eV)**	-238	from -50 to -220	-264
$E_{sq/hq}$ **(eV)**	-172	from -370 to -450	-255

This fundamental difference can be explained by the negative electrostatic environment around the FMN in typical Flds, which is replaced by a more neutral or positively charged environment in the case of NrdIs from *Bacillus subtilis* and *E. coli*, respectively. The negative electrostatic environment in typical Flds is proposed to hinder reduction of sq to hq, hence lowering $E_{sq/hq}$ [Bennett-Lovsey et al., 2008; Cotruvo and Stubbe, 2008; Johansson et al., 2010; Kelley, MacCallum and Sternberg, 2000; Zhou and Swenson, 1995]. Interestingly, a substitution of aspartate residue number 95 with an asparagine residue, thus converting this residue from a negative to a neutral one; in oxidised Fld from *Desulfovibrio vulgaris* increased $E_{sq/hq}$ by 46 mV. Because this residue, which is 6.3 Å from the flavin N(1), is conserved as a D in most Flds and as an N in all NrdIs, it is proposed to play an important role in the destabilisation of the sq form of flavin mono dinucleotide (FMN) observed in *E. coli* NrdI [McCarthy et al., 2002; Cotruvo and Stubbe, 2008]. Moreover, the elevated $E_{ox/sq}$ level in NrdI may be explained by the presence of a flexible, glycine-rich loop in the vicinity of N(5) in of the FMN of most NrdIs, which is proposed to stabilise the ox form of flavin with its nonpolar and neutral properties [Cotruvo and Stubbe, 2008; Drennan et al., 1999; Hoover et al., 1999 and Ludwig et al., 1997].

Generation of an active cofactor in class Ib RNRs. A model of the mechanistic pathway for the generation of an active cofactor in class Ib RNRs has been developed [Cox et al, 2010; Cotruvo and Stubbe, 2010]. The reaction mechanisms is based on a cofactor with manganese, and use either hydroperoxides (HO_2^-) or hydrogenperoxides (H_2O_2) to oxidise $Mn^{II}Mn^{II}$ and to extract an electron and a proton from tyrosine, resulting in the $Mn^{III}Mn^{III}$-Y• cofactor (**Figure 1.3b**) [Cox et al, 2010; Cotruvo and Stubbe, 2010; Tomter et al., 2012]. Structural studies have revealed that upon complex formation between NrdI and NrdF, the active site channel in NrdF is extended towards the flavin ring in NrdI, defining a path from the FMN site in NrdI to the Mn site of NrdF. Moreover, a trapped species, which was best modelled as (the putative) peroxide, was observed in this channel. This finding supports the proposed mechanism of $Mn^{III}Mn^{III}$-Y• assembly [Boal et al., 2010]. The fact that *E. coli* NrdI seems to have been fine-tuned for a rapid transfer of its second electron, and thereby ensures effective delivery of two electrons in two one-electron transfers [Cotruvo and Stubbe, 2008], further supports the proposed mechanism. Whether NrdI is present in stochiometric amounts relative to NrdF, or if an Fld reductase (FldR) allows NrdI to function catalytically, remains to be established. However, the discovery of NrdI and its function have shed new light to a previous electron spin resonance study [Khangulov et al., 1990]. The study reveals that *in vitro* assembled

manganese-enzyme from *Thermus thermophilus* showed an activity level doubled compared to that of *in vitro* assembled iron-enzyme, and that the cofactor-to-protein ratio (Y•/β_2) was approximately three times higher for the iron-enzyme. Viewed from the point of the proposed reaction mechanism, the finding that the class Ib RNR has a low Y• content, may result from a requirement of additional components in the system. An NrdI reductase could to facilitate the supply of peroxides for the mechanism and to re-reduce NrdI for multiple catalytic cycles [Cotruvo and Stubbe, 2011b].

1.3. Aims of the study

The focus of this master project has been on two FldRs encoded by *B. cereus*. Recent discoveries have proposed that the radical generating component of the class Ib RNR system, i.e. the metal cofactor in the NrdF subunit, is a dimanganese-cluster instead of a diiron-cluster. It has further been shown that the flavoprotein NrdI is essential for the generation of the tyrosyl radical when the metal is manganese. Hence, for a functional class Ib RNR system (with manganese), the NrdI itself needs to be reduced. Since NrdI is a flavodoxin-like protein, the most probable reductant for NrdI would be a FldR. Two FldRs have been identified in the genome of *B. cereus*, and the aim of this master project was to investigate them (**Figure 1.9**). They are of the approximate same size, BC0385 is of 39 kD and BC4926 is of 36 kD, and the sequence identity is 41 %. Therefore, they are assumed to have similar functions *in vivo*. The goal was to be able to reveal if either FldRs could reduce NrdI, if a specific reductase is needed for this purpose and if one of these FldRs is that specific reductase. Such findings would enhance the knowledge about the function of NrdI, which still is unclear, and thus also tell more about the enzymatic process of ribonucleotide reduction in the class Ib RNR system, in *B. cereus*, specifically.

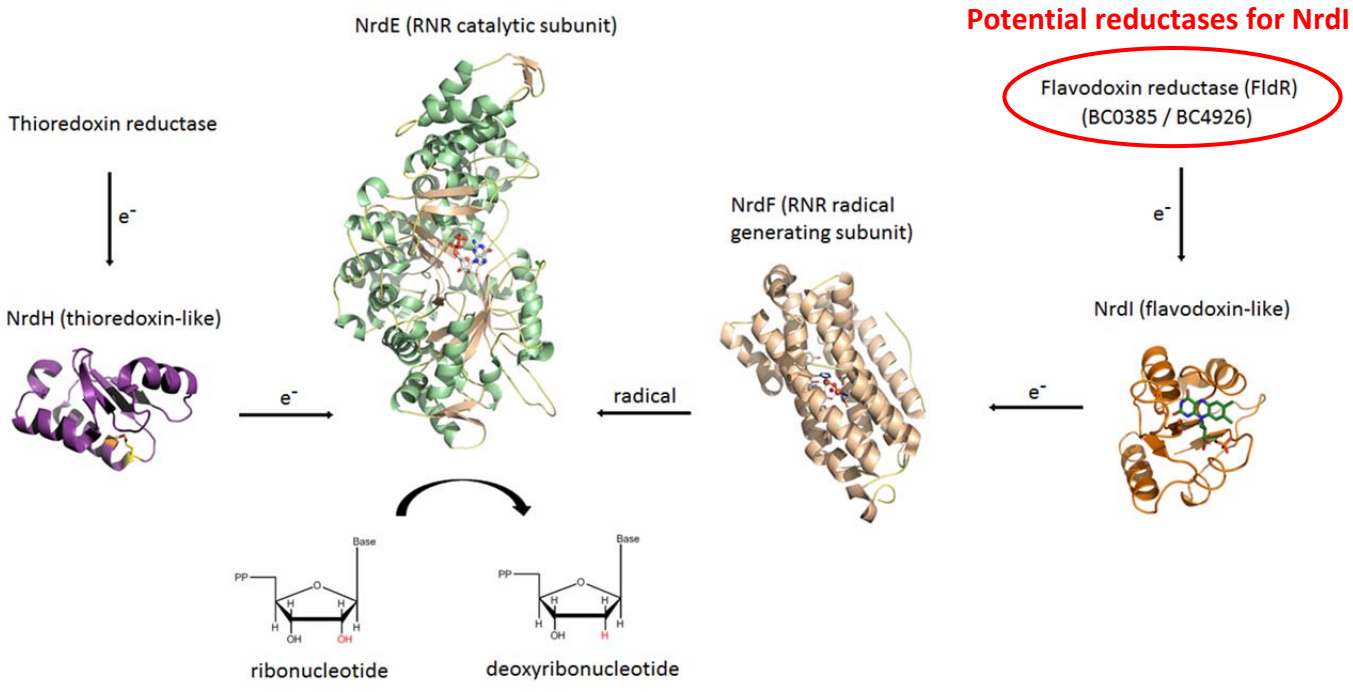

Figure 1.9: The class Ib RNR system in *B. cereus*. Two potential FldRs have been located in the genome of the species; FldR BC0385 and FldR BC4926 (red ring).

The investigation of the FldRs involves both their activities and their structures, and involves the following key goals:

- **Generation of FldR BC0385 expressing *E. coli* cells**
  Design primers to amplify BC0385 from *B. cereus* genomic DNA, clone the gene into a pET-22b expression vector, transform *E. coli* cells with the plasmid
- **Express and purify both FldRs**
  Growth, expression and purification of each FldR; develop a purification protocol for each FldR
- **Measure redox activity levels for both FldRs**
  Activity assays with each FldR; activity assays with each FldR and NrdI, respectively
- **Crystallise both FldRs; co-crystallise each FldR with NrdI**
  Screen for crystallisation condition(s) for each FldR, optimise the conditions, grow large crystals from these conditions and perform X-ray diffraction experiments on the crystals
- **Solve the crystal structures of FldR BC0385 and FldR BC4926**
  Use the data sets from the X-ray diffraction experiments to solve the crystal structures of the FldRs

1.4. Protein X-ray crystallography

One of the main aims of this project was to solve the 3D-structure of the two FldR candidates. Protein crystallography is a powerful method that allows for determination of the crystal structure of proteins. Only the first steps of protein crystallography was used in this master project, and they are briefly introduced below.

1.4.1. Protein X-ray crystallography

Protein X-ray crystallography (PX) can be looked on as an analogue to a microscope. The maximal resolution the microscope gives, is limited by the wavelength of the radiation used. A light microscope is e.g. based on the scattering of visual light, and cannot resolve details that are closer together than half the wavelength of visible light, which ranges from~400 nm to~700 nm [Lattman and Loll, 2008].

The distances between atoms in a molecule are typically 0.8-2.5 Å (0.08-0.25 nm; **Figure 1.10**). As X-rays have wavelengths between 0.5 Å and 1.6 Å, they can be used to visualise protein molecules and the sub-molecular details in them [Blow, 2002].

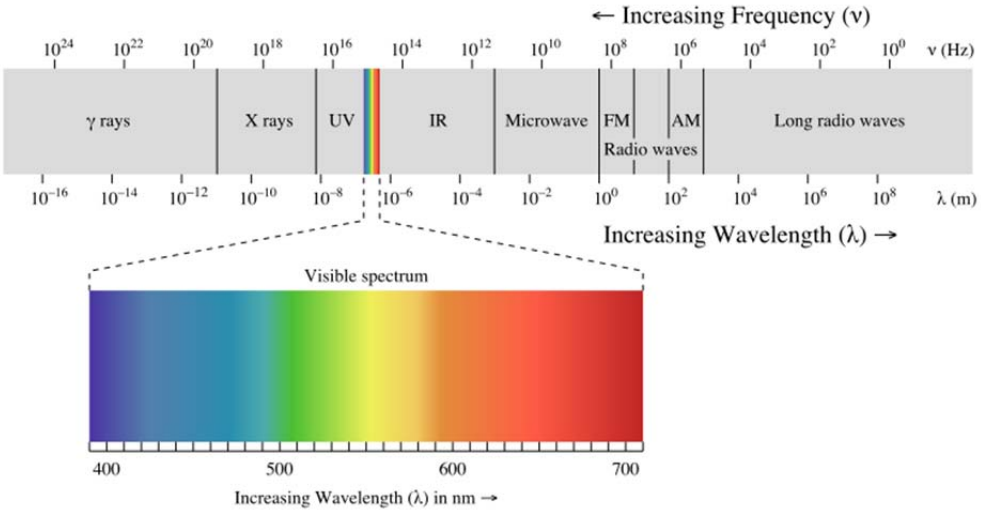

Figure 1.10: The spectrum of electromagnetic rays (light). Visible light ranges from~400 nm to~700 nm; X-rays ranges from~0.05 nm to~0.16 nm. The figure is taken from Wikipedia.

1.4.2. Scattering

Scattering, or diffraction, is the process by which matter deflects light rays from their straight lined path, without change of wavelength. In microscopy, light scattered by the specimen is captured and focused by lenses to make an image. In PX, the light (X-rays) scattered by the protein crystal is captured by a detector. An image of the protein is obtained by performing calculations that mimic the action of the lens [Lattman and Loll, 2008].

When an X-ray photon encounters an electron, it may be absorbed, and if so, the electron is set into vibration at the X-ray frequency. This vibrating electron then emits an X-ray photon of the original energy and wavelength [Blow, 2002].

1.4.3. The nature of protein crystals and crystal growth

To determine the structure of a protein molecule, the scattering effect from one single molecule is not enough. Under the right conditions, protein molecules can pack together with a high degree of symmetry. In principle, each molecule of the three-dimentional protein crystal provides a copy of the same signal, thus enhancing the diffraction pattern and making it possible to visualise the protein molecule [Blow, 2002].

Crystallisation of proteins is based on bringing the protein solution into a supersaturated state (**Figure 1.11**). Factors such as pH and temperature, as well as concentration and type of salt and hydrophobic polymers, can affect protein solubility. The extents of the affection depend on the properties of the specific protein [Weber, 1997]. An example of a phase diagram of a protein is presented in **Figure 1.11**, where protein concentration is a function of salt concentration. The curves define the different levels (zones) of supersaturation, which in turn determines at which protein and salt concentrations crystals are obtained. The level of supersaturation also determines what kind of protein crystals that are grown [Drenth, 1999]. If the level of supersaturation is in the area of nucleation, protein molecules accumulates to form small protein aggregates. These aggregates serve as nuclei for crystal growth. To obtain a few, large crystals in stead of many small, it is necessary to achieve crystal nuclei in the nucleation zone, followed by transition to the growth zone. The growth zone possesses a lower degree of supersaturation, which supports crystal growth in stead of formation of more nuclei [Weber, 1997].

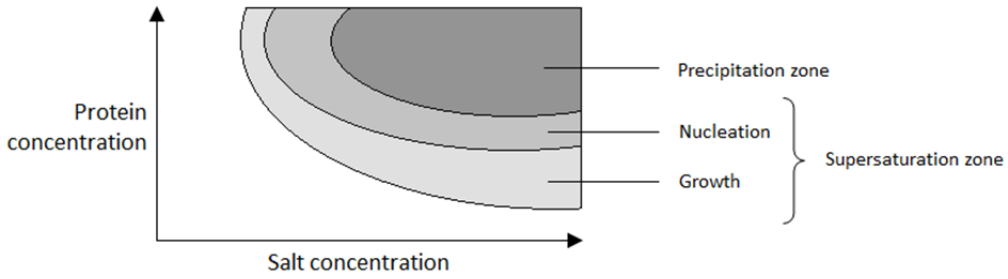

Figure 1.11: Typical solubility curves in the phase diagram of a protein. Crystal nucleation is a critical phenomenon that occurs only in the supersaturation zone. Crystals grow under conditions of supersaturation after nuclei have taken form. A typical path for obtaining a few, large crystals, is presented as red arrows.

1.4.4. Vapour diffusion

The most frequently used crystallisation methods are the vapour diffusion techniques. The *reservoir solution* contains buffer, salt and eventually other additives. A droplet containing a mix of protein solution and reservoir solution is equilibrated against the reservoir solution in a defined, closed environment. The difference in precipitant concentration is driven towards equilibrium through vapour diffusion, which leads to a slow decrease of protein droplet volume and thus a slow increase of protein concentration in the droplet. Under the right conditions, the concentration is increased into the nucleation zone and thereafter decreased into the growth zone, and a few, large crystals are obtained. Two types of vapour diffusion setups are presented in **Figure 1.12**; namely hanging drop and sitting drop.

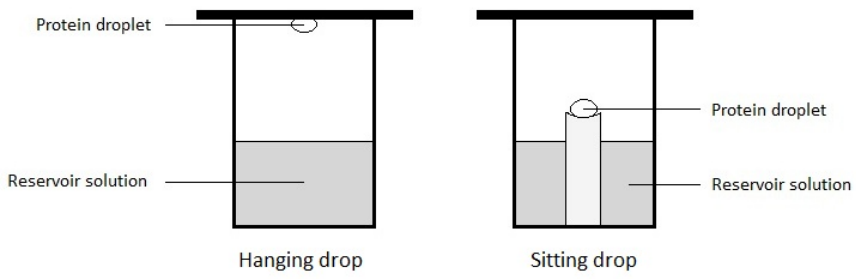

Figure 1.12: Two types of vapour diffusion setup.

2. Methods

Presented here are the methods used to study the two proteins of interest, i.e. the two (potential) FldRs – BC0385 and BC4926 – which are encoded in the genome of B. cereus. First, it is described how the generation of FldR BC0385-expressing cells was performed, which included the polymerase chain reaction (PCR) for amplification of the *BC0385* gene, restriction cutting of the insert (the gene) and the vector with subsequent ligation of the two DNA molecules, and transformation of competent *E. coli* cells with the ligation product. Thereafter, a standard procedure was developed for the expression and purification of the two proteins, followed by procedures for crystallisation of the proteins, X-ray diffraction experiments and measurement of protein activity.

2.1. Cloning of *BC0385* into the pET-22b expression vector and generation of FldR BC0385 expressing *E. coli* cells

In this project, the expression vector pET-22b was utilised to facilitate (over)expression of both FldRs. In the pET system, target genes are expressed from the plasmid under control of T7 polymerase transcription. Transcription of both T7 polymerase and the gene of interest is activated by the presence of Isopropyl-β-D-Thiogalactopyranoside (IPTG) [Novagen, 2010]. For one of the FldRs it had previously been developed an expression system with the pET-22b vector and *E. coli* BL21 (DE3) cells, and a similar expression system had to be developed for the other FldR.

2.1.1. Amplification of *BC0385*

PCR was performed to generate *BC0385* DNA fragments for subsequent cloning into the pET-22b expression vector. The DNA sequence of the pET-22b vector contains restriction sites for a number of restriction enzymes; in the process of amplifying a gene by the use of PCR, it is possible to introduce the same restriction sites flanking the gene which is subjected

to cloning. This is performed by designing primers containing these restriction sites, which is then used in the PCR.

A small sample of the provided stock of *B. cereus* ATCC 14579 was spread onto agar plates (Table A4.2) in a sterile environment and incubated at 37 °C for 15 hours. A 3 ml Luria Broth (LB) culture was made from one of the largest single colonies and incubated at 37 °C with 250 rpm shaking until a 1:4-dilution of the culture had reached OD_{600} = 0.90. Plasmid was purified from the culture using the NucleoSpin plasmid kit with a slightly modified protocol (spinning down 3 µL of cell culture instead of 1 µL; eluate with 35 µL instead of 50 µL in the final step). The concentration of *B. cereus* genomic DNA in the sample was measured using NanoDrop (ND-1000, Nanodrop Technologies).

Forward and reverse primers with NdeI and HindIII restriction sites were designed for BC0385 (section A5.3.).

PCR was performed with the primers designed for BC0385 and *B. cereus* genomic DNA as template using a gradient for the annealing temperature (Table A2.1). The size of the PCR product from the eight different reaction mixtures was tested and purified by agarose gel electrophoresis with a 0.8 % gel (Table A4.1). The bands containing DNA fragments of the size corresponding to the length of *BC0385* (1050 base pairs) were excised from the gel and further purified using the Wizard SV Gel and PCR Clean-Up System kit. The concentration of PCR product in the sample was measured using NanoDrop.

2.1.2. Purification of pET-22b vector

Amplification and purification of pET-22b expression vector was performed, in order to generate a sample with a vector concentration suitable for the process of cloning the *BC0385* into the vector.

A small sample of the provided stock of *E. coli* bacterial strain TOP10 containing the pET-22b vector was spread onto agar plates (100 µg/mL ampicillin) and incubated at 37 °C for 15 hours. 6 parallels of 6 mL LB cultures (100 µg/mL ampicillin) were made from each of the 6 largest single colonies and incubated at 37 °C and 250 rpm for 17 hours. Plasmid was purified from the cultures using the NucleoSpin plasmid kit, with a somewhat modified protocol due

to initial difficulties in getting a high enough concentration of plasmid in the sample (section A.6.1). The concentration of pET-22b vector in the sample was measured using NanoDrop.

2.1.3. Restriction cutting and ligation of BC0385 and pET-22b vector

The plasmid and the DNA fragment of the gene to be cloned are cut with the same two restriction enzymes to introduce compatible ends in the respective molecules, which subsequently can be ligated together. By using two different restriction enzymes in stead of one, it is made sure that the gene (or DNA fragment) is inserted into the vector in the appropriate direction.

The PCR product from the amplification of *BC0385* and the prepared pET-22b vector were separately double digested with restriction enzymes NdeI and HindIII and incubated in a 37 °C water bath for 1 hour (Table A3.1). The FastDigest buffers and enzyme solutions were used since they turned out to give positive results (Table A3.1). After the normal (i.e. not *Fast*-) buffers and enzyme solutions was tried out with different incubation times and temperatures, but gave only negative results. The digestion products were purified by agarose gel electrophoresis with a 0.8 % gel (Table A4.1). The bands containing DNA fragments of the size corresponding to the length of pET-22b (5493 base pairs) and *BC0385* (1050 + 4 from primers = 1054 base pairs) were excised from the gel and further purified using the Wizard SV Gel and PCR Clean-Up System kit. The concentrations of PCR-product and pET-22b vector in the samples were measured using NanoDrop.

The purified digestion products were ligated with T4 ligase and a 3 times molar excess of BC0385 in room temperature for 1 hour (Table A3.2).

A small amount of the ligation product was analysed by agarose gel electrophoresis to ensure that the plasmid corresponded to the length of pET-22b with the *BC0385* insert (6547 base pairs).

2.1.4. Transformation of competent hosts with the ligation product

E. coli XL10-Gold ultracompetent cells are created for transformation of large DNA molecules with high efficiency. These cells were transformed with the ligation product as follows.

1) Thaw the cells on wet ice for 5 minutes

2) Add 5 µL of ligation mixture and incubate on ice for 30 minutes

3) Heat shock the cells in a 42 °C water bath for 1 minute

4) Cool down the cells on wet ice for 2 minutes

5) Add 900 µL SOC medium which are pre-heated to 42 °C and incubate in a 37 °C water bath for 30 minutes.

A small sample of the transformation mixture was spread onto agar plates (100 µg/mL ampicillin) and incubated at 37 °C for 15 hours. A 3 mL LB culture (100 µg/mL ampicillin) was made from one of the largest single colonies and incubated at 37 °C and 250 rpm for 17 hours. Plasmid was purified from the culture using the NucleoSpin plasmid kit with the same modifications of the protocol as before. The concentration of plasmid in the sample was measured with NanoDrop.

The plasmid was sequenced in three parallels at the ABI-lab at the University of Oslo (sample details in Appendix 5).

2.1.5. Site-directed mutagenesis

To back-mutate a so-called missense mutation – i.e. a mutation leading to amino acid substitution in the gene product – that had occurred in the *BC0385* sequence during PCR, the vector with the mutated insert was subjected to design of mutagenic primers and subsequent PCR with these.

Forward and reverse primers mutagenic for the substituted base pair number 114 in *BC0385* were designed and ordered (section A5.4.), and PCR was performed with the primers and the ligation product as template (Table A2.2).

DpnI endonuclease has the target sequence 5'-Gm6ATC-3' and is used to remove template DNA. Because the newly synthesised DNA molecules from the PCR are not methylated, this is an efficient method to remove the template, which is not wanted to be a participant in cell transformation [Weiner et al., 1994].

To destroy the template, 1 µL of *DpnI* (10 u/µL) was added directly to the PCR tubes after the end of the PCR program and the mixture was incubated for 1 hour at 37 °C. A small amount of the PCR product was analysed by agarose gel electrophoresis with a 0.8 % gel (Table A4.1) to ensure that the DNA was of the right size (6547 base pairs).

E. coli XL10-Gold ultracompentent cells were transformed with the PCR product after the same protocol as for the ligation product (section 2.1.4.), but in step 2) 10 µL PCR mixture was added instead of 5 µL ligation mixture.

A small sample of the transformation mixture was spread onto agar plates (100 µg/mL ampicillin) and incubated at 37 °C for 15 hours. A 3 mL culture (100 µg/mL ampicillin) was made from one of the largest single colonies and incubated at 37 °C and 250 rpm for 17 hours. Plasmid was purified from the culture using the NucleoSpin plasmid kit with the same modifications of the protocol as before. The concentration of plasmid in the sample was measured with NanoDrop.

The plasmid was sequenced at the ABI-lab at the University of Oslo in six parallels; three using the T7 polymerase and three using the T7 terminator polymerase (sample details in section A.5.1.).

2.1.6. Transformation of expression hosts with the plasmid

E. coli BL21 (DE3) competent cells are developed with regard to effective protein expression.

E. coli BL21 (DE3) competent cells were transformed with the plasmid (i.e. the pET-22b vector with inserted *BC0385*) after the same protocol as for the ligation product (section 2.4.1.), but in step 2, 3 µL plasmid sample was added instead of 5 µL ligation mixture.

A small sample of the transformation mixture was spread onto agar plates containing 100 µg/mL ampicillin and incubated at 37 °C for 15 hours. A 200 mL LB culture (100 µg/mL ampicillin) was made from one of the largest single colonies and incubated at 37 °C and 250

rpm for 17 hours. 4 mL LB culture was diluted in a new 200 mL LB culture (100 µg/mL ampicillin) and incubated for 7 hours at 37 °C. Stocks were made by mixing 500 µL of LB cultured cells with 500 µL glycerol (60 %) and stored at -80 °C.

2.2. Expression and purification of FldR BC0385 and FldR BC4926

A stock of *E. coli* cells of the strain BL21 (DE3), containing a vector with the *BC4926* gene inserted, was previously generated, and kindly provided, by Åsmund K. Røhr. Possessing *E. coli* cells expressing both FldRs, respectively, the next step was to produce and purify the two proteins for subsequent crystallisation experiments and activity measurements.

The following procedure of expression and purification applies for both FldR BC0385 and FldR BC4926, if not specified otherwise.

2.2.1. Growth of FldR expressing *E. coli* cells

A small sample of the freeze stock of FldR-expressing *E. coli* was spread onto agar plates (100 µg/mL ampicillin) and incubated at 37 °C for 15 hours. A 200 mL LB culture (100 µg/mL ampicillin) was made from one of the largest single colonies and incubated at 37 °C and with 250 rpm shaking for 17 hours. 4 mL of this LB culture was diluted in a new 200 mL LB culture (100 µg/mL ampicillin) and incubated for 7 hours at 37 °C. 6 x 10 mL samples of the new LB culture was then diluted in 6 x 1000 mL Terrific Broth (TB) cultures (100 µg/mL ampicillin) and incubated at 37 °C and 250 rpm until $OD_{600} = 0.9 \pm 0.1$ (for about 2-3 hours). The TB cultures were then put on ice until the temperature had dropped to 20 °C. A 50 µL sample was taken from one of the TB cultures for an expression test (section 2.2.2.), centrifuged for 1 min at 19,000 *g* and stored at -80 °C. Over-expression of FldR in the 6 cultures was induced with 1 mM IPTG and they were incubated at 20 °C and 250 rpm for 14 hours. A 25 µL sample was taken from one of the cultures for the expression test (see below), centrifuged for 1 min at 19,000 *g* and stored at -80 °C. Bacteria was harvested at 5000 *g* for 15 minutes, and the bacteria paste was divided into samples of approximately 15 g and stored in zip lock plastic bags at -20 °C.

2.2.2. Testing the expression of FldR

The protein content of the TB culture before and after induction of over expression (and subsequent growth for 15 hours) was analysed by sodium dodecyl sulphate polyacrylamide gel electrophoresis (SDS-PAGE). This was to investigate if the *E. coli* cells actually expressed the FldRs.

The pellets from the 50 µL and 25 µL TB culture samples were suspended in 50 µL and 100 µL protein cracking solution (Table A4.3), respectively. The samples were vortexed, heated to 90 °C for 2 minutes and vortexed again. 1 µL of each mix was applied to a 10-15 % gradient gel for SDS-PAGE, and subject to a pre-programmed separation script on the PhastGel system, specific for the gradient in the gel.

2.2.3. Lysis of FldR expressing *E. coli* cells

The cell walls of bacteria have a rigid layer, called peptidoglycan, which is primarily responsible for the strength of the wall. In gram-negative bacteria, such as *E. coli*, an additional layer is present outside the rigid layer, called the outer membrane or the lipopolysaccharide layer. Due to this rigidity, a high pressure is required to rupture the cell wall of *E. coli* cells [Mardigan and Martinko, 2006]. The principle of the X-press® is to break frozen cells by squeezing them through a small opening under high pressure, which will disrupt the cell wall and membrane [Magnusson and Edelbo, 1976].

Approximately 15 g of bacteria paste was cooled down with N_2 (l) and thoroughly crushed before applied to the X-press equipment, which had been pre-cooled to -20 °C. The equipment was put together and the bacteria were lysed by being pushed back and forth through a tiny hole by the use of an air compressor.

From this point and through the rest of the purification process, it was made sure that the protein solution was kept at 4 °C by working in a 4 °C room or on ice, pre-chilling solutions before applying them to the protein solution as well as using a centrifuge cooled to 4 °C. The protein solution was stored at -20 °C during longer halts in the purification procedures.

The lysed bacteria were dissolved in 100 mL buffer A (Table A4.4) over a time period of 30 minutes, and thereafter centrifuged at 39,000 *g* for 1 hour. The supernatant was kept for the next step.

2.2.4. Purification of FldR: DNA precipitation

Added in small increments to solutions of low ionic strength, streptomycin (first) precipitates DNA [Cohen and Lichtenstein, 1960]. Therefore, as the first step in the protein purification process, Streptomycin sulphate was used to remove DNA from the solution.

A 10 % streptomycin sulphate solution corresponding to ¼ of the supernatant was added over a period of 5 minutes while stirring at low speed on a magnetic stirrer, before subsequent stirring at low speed for another 10 minutes. The solution was centrifuged at 39,000 *g* for 30 minutes and the supernatant was kept for the next step.

2.2.5. Purification of FldR: Protein precipitation by salting out

At high ionic strengths, the solubility of proteins decreases. When the salt concentration in a protein solution is increased, the solvent is becoming occupied in polar interactions with the ions, i.e. solvating the salt ions. The reduced amount of solvent available to engage in interactions with the protein, i.e. solvate the protein, causes the protein to precipitate. The precipitation of proteins caused by the formation of hydrophobic interactions with each other is often executed by the use of ammonium sulphate ($(NH_4)_2(SO)_4$). The salt concentration at which a protein precipitates differs from one protein to another. Hence, salting out can be used to fractionate proteins [Voet and Voet, 2004].

A specified amount of $(NH_4)_2(SO)_4$ salt per mL supernatant was added over a period of 15 minutes on a magnetic stirrer and stirred at low speed for another 20 minutes; 0.43 g/mL for the FldR BC0385 and 0.22 g/mL for the FldR BC4929. After precipitation the solution was centrifuged at 39,000 *g* for 20 minutes, and the protein pellet was kept for the next step.

This purification step had previously been optimised with respect to FldR BC4926 showing that 0.22 g $(NH_4)_2(SO)_4$ per mL supernatant was enough to salt out all the FldR BC4926 protein from solution. With respect to the FldR BC0385, the required amount of $(NH_4)_2(SO)_4$ was not optimised because of time limitations; a standard amount of 0.43 g/mL was chosen.

From this point and through the rest of the purification process, it was made sure that no bubbles were generated in the protein solution, as this could lead to protein denaturation.

2.2.6. Purification of FldR: Desalting chromatography

Prior to anion exchange chromatography, desalting chromatography (low resolution size exclusion chromatography) of the protein sample was performed in order to lower the salt concentration (see section 2.2.9. for principle). Proteins in general absorb light at 280 nm [Voet and Voet, 2004], and this property was used to monitor the proteins in this purification step.

The pellet was dissolved in 10 mL Buffer A (Table A4.4.) over a period of 1-2 hours, with gentle stirring and pipetting now and then. The protein solution was filtered through a 0.22 µm filter before subsequent desalting on a 2 x 5 mL HiTrap desalting column on the Äkta purifier system. The sample was eluted with Buffer A (Table A4.4), and the fractions showing absorption at 280 nm and low conductivity were collected for further purification.

2.2.7. Purification of FldR: anion exchange chromatography

Ion exchange chromatography is a method used to separate proteins according to differences in charge and charge distribution. The separation is based on the reversible adsorption of charged protein molecules to immobilised groups in the column material, and these groups have a charge opposite to that of the protein molecules. When negatively charged proteins are adsorbed to a positively charged column material, they can be released by gradually increasing the concentration of salt (e.g. potassium chloride) in the elution buffer. Then the chloride ions will compete with the proteins in binding to the positively charged column material, and the proteins with a low density of net negative charge will tend to emerge first, followed by those having a higher negative charge density [Berg, Tymoczko and Stryer, 2007]. Proteins in general absorb light at 280 nm, and flavins absorb light at 450 nm in their oxidised state [Massey, 2000], and these properties were used to monitor the flavin-containing FldR proteins in this purification step.

Protein fractions from desalting chromatography were filtered through a 0.22 µm filter before subsequent purification on a Q HP anion exchange column. The protein was eluted with buffer B (Table A4.4), and by increasing the salt concentration with a linear gradient using buffer C (Table A4.4). The fractions showing absorption at both 280 nm and 450 nm were collected for further purification.

As a part of developing a standard procedure, the pH in the protein sample and in the ion exchange buffers (Buffer B and Buffer C) was increased until the protein was negatively charged and hence adsorbed to the column material.

To further optimise the standard procedure, the salt gradient was adjusted to go from 0 % and to an upper value defined by the point where all the protein of interest had been eluted. A part of this was also to choose a gradient length which gave a good separation without being too time consuming.

The collected fractions were analysed by SDS-PAGE to confirm the size of the protein in the collected peak(s) to see if it corresponded to the calculated size of the FldR. A small sample of the protein solution was mixed 50:50 with protein cracking solution, and the rest of the procedure is previously described in section 2.2.2. The fractions containing the protein of interest were pooled and kept for further purification.

Reconstitution of FldR BC4926 from apo protein and flavin

Before further purification, FldR BC4926 was tried reconstituted from apo-FldR and flavin.

First, to determine if apo-FldR binds either FMN or FAD, a small sample (2 mL) of apo-FldR from anion exchange chromatography was divided in two equal samples (1 mL); these were each mixed with one of the two flavin cofactors, FAD and FMN, respectively, to a concentration of 1 mM. Each sample was filtered through a 0.22 μm filter before subsequent purification on a 2 x 5 mL HiTrap desalting column to determine the amount of cofactor that bound to the FldR.

The flavin cofactor which appeared to bind most effectively was used to reconstitute higher quantities of protein, but this time with cofactor to a concentration of 0.1 mM. The reconstituted protein was purified by gel filtration chromatography (section 2.2.9.).

2.2.9. Purification of FldR: Gel filtration chromatography

Gel filtration chromatography is, like desalting chromatography, size exclusion, but with a higher resolution. The column consists of porous beads made of a polymer; small molecules can enter these beads, but large ones can not. The result is that small molecules are distributed

in the aqueous solution both inside the beads and between them, whereas large molecules are only located in the solution between the beads. Hence, large proteins are eluted from the gel filtration column before smaller proteins [Berg, Tymoczko and Stryer, 2007].

The collected protein solution from the anion exchange chromatography was concentrated using an Amicon ultrafiltration cell containing a filter with a cut-off value of 30,000 Da. Due to precipitation of the FldR and the reconstituted FldR, the protein solution was concentrated until protein almost started to precipitate. Samples of 25-50 µL were applied to a Sephadex G75 gel filtration column eluted with Buffer D (Table A4.4). Fractions absorbing light at 450 nm were collected.

2.3. Crystallization of FldR BC0385 and FldR BC4926

Protein crystallisation can be thought of as a two-stage process; 1) identify one or more conditions in which a certain protein precipitates as ordered crystals and 2) optimise the condition(s) to produce protein crystals of a quality that makes them suitable for X-ray diffraction experiments. To identify conditions in which a protein crystallises, different buffers, pH values, precipitants, temperatures and crystallisation methods are usually varied in a systematic or a random way, referred to as screening. The different parameters usually affect the outcome to a large extent, both when it comes to if crystals are obtained or not, and when it comes to the shape and quality of the crystals that are eventually obtained.

2.3.1. Screening for crystallisation conditions

The vapour diffusion technique with a sitting drop setup was used to screen for crystallisation conditions. All the screening was performed at the Oryx 6 Robot (kindly provided by the group of Magnar Bjørås at OUS Rikshospitalet, Oslo, Norway) by the use of different commercial crystallisation screens (Table A1.7). The screens have typically 96 different conditions with varying precipitants, pH and additives. Crystallisation trays with two drops for each condition were used; concentrated protein was deposited as the first drop while the second drop normally had lower protein concentration. The different screens used in the

screening experiments with the different FldRs are presented in **Table 2.3.1**, as well as the content of protein and eventual other diluents in the second drop.

Normally, the protein solution after gel filtration was concentrated until protein precipitation was barely indicated. The protein solution was then centrifuged at 19,000 *g* for one minute and precipitated protein was discarded before the screening was performed. In the case of apo-FldR BC4926, the protein solution after gel filtration was concentrated to ~15 mg/mL in one screening experiment and to 60 mg/mL in a separate screening experiment.

Table 2.3.1: The different screens and the content of the second drop in the screening experiments with the different FldRs.

Protein	**Screens**	**Content of second drop**
FldR BC0385	JSCG+ and Index	50 % protein
FldR BC4926, reconstituted	JSCG+, Natrix (E-H) and PEG/Ion(A-D) and Wizard I+II	100 % protein and a small excess of FAD
apo-FldR BC4926 (~15 mg/mL)	JSCG+, PEG/Ion and Wizard I+II	50 % protein
apo-FldR BC4926 (~60 mg/mL)	JSCG+ and Midas	50 % protein
FldR BC4926	Index, JSCG+ and Wizard I+II	Buffer*

* A second drop was not set up because of limited amounts of protein solution.

The conditions resulting in hits (e.g. small crystals) were tried optimised for the growth of large crystals by varying the protein and precipitant concentration in a systematic way.

2.3.2. Optimisation of crystallisation conditions for apo-FldR BC4926

The condition in well H11 in the Wizard I+II screen (details in Table A.4.5) was tried optimised for the most diluted sample of FldR BC4926 apo form. The concentrations of zinc acetate ($ZnAc_2$) and protein were both varied between 25 % and 100 %, in separate experiments.

The conditions in wells H10 and H11 in the Wizard I+II screen (details in Table A.4.5) was further investigated for the 15 mg/mL sample of FldR BC4926 apo form. The concentrations of polyethylene glycol (PEG) and protein were varied separately between 25 % and 100 %. This was performed in two parallels for both the H10 and H11 conditions; one parallel at room temperature and one parallel at 4 °C. In addition, two experiments with 50 % and 25 % protein were set up for the H10 condition, respectively, both with PEG concentration reduced to 25 %.

2.3.3. Optimisation of crystallization conditions for FldR BC4926

The conditions in wells A7 and B3 in the JSCG+ (details in Table A.4.6) screen was further investigated. The concentrations of PEG and protein were varied separately at 4 °C.

2.4. X-ray diffraction, data collection and data processing

Prior to X-ray diffraction experiments each of the crystals were transferred into a cryo solution containing the crystallization solution (70%) mixed with glycerol (30 %) as antifreeze before subsequent freezing in liquid nitrogen.

The X-ray diffraction experiments were performed at beam line ID29 at the European Synchrotron Radiation Facility (ESRF), Grenoble, France and at beam line X10SA at the Swiss-Light Source (SLS), at Paul Scherrer Institut (PSI), Villigen, Switzerland.

The diffraction images from the initial experiments were indexed with MOSFLM and the space group determined with POINTLESS [Leslie and Powell, 2007; Evans, 2005].

2.5. Activity measurements

2.5.1. Determination of the specific activity of the FldRs with DCPIP

In order to compare the activity of the two FldRs, the ability of each FldR to catalyse the reduction of 2,6-dichlorophenolindophenol (DCPIP) with NADH as electron donor was determined. The reduction of DCPIP can be measured spectroscopically; it has a light absorption maximum at 600 nm wavelength in its oxidised state, but in its reduced state it exhibits no absorption at this wavelength [Armstrong, 1965]. Thus, the electron transfer from NADH via FldR to DCPIP can be determined by measuring the drop in absorption at 600 nm (A_{600}). The setup and the procedure were based on standard procedures by Worthington Biochemical Corporation (2012).

The initial velocity of DCPIP reduction was measured at different DCPIP concentrations as follows. Because the reduction of DCPIP by NADH takes place also in the absence of a catalyst [Dupuy, 2004], two parallels were measured for each reaction, one with FldR and one without. During the calculations, the amount of DCPIP reduced in the absence of FldR was subtracted from the amount that was reduced in the presence of FldR.

1) Mix Tris·HCl buffer (200 mM, pH 8.0) and DCPIP (different concentrations, ranging from 4 μM to 800 μM) in an eppendorf tube
2) Start the timer at the moment NADH (300 μM) is added to the tube
3) Add water (for blind reaction) or FldR (0.42 μM) to the tube
4) Mix the components by pipetting up and down one time, and transfer the solution to a cuvette
5) Measure the light absorption of the solution for the first time when the timer shows 30 seconds, and measure a new absorption spectrum every 15 seconds during 240 seconds
6) Repeat the procedure with a different concentration of DCPIP

A_{705} and A_{800} was measured in addition to A_{600}. For a specific A_{600} around 1 absorbance unit (AU), it was observed that A_{705} was 1/5 of this value. This knowledge was used when the concentration of DCPIP gave absorption values exceeding 1.5 AU; the A_{705} was multiplied with 5 and reported as A_{600}. DCPIP does not absorb any light at 800 nm. By measuring A_{800}, it was ensured that the different spectra had the same base line.

The initial velocity (V_0) of each reaction was determined (by "initial velocity" it is meant the velocity in the time range which the reaction was linear). The velocity was plotted against the concentration of DCPIP for each reaction in the series of different concentrations, and Origin (Origin 8.6, OriginLab Corporation) was used to estimate a Michaelis-Menten curve fit for the plot.

Before the experiment was carried out, the effects of different buffer concentrations and pH values were investigated, as well as the presence and absence of zinc chloride ($ZnCl_2$), which was a part of the original setup. This was done in order to optimise the reaction conditions with regard to the functionality of the FldRs.

2.5.2. Comparison of the FldR activities with cytochrome c

In order to compare the reducing effect each FldR has on a different substrate, the reduction of cytochrome *c* (Cyt*c*) with NADPH as the electron donor was tested after inspiration from Leadbeater et al. (2000). The reduction can be determined by measuring the increase in light absorption at 550 nm, as only Cyt*c* in its reduced form exhibits absorption at this wavelength [Krab and Wikström, 1979].

Phosphate buffer (10 mM, pH 8.0), Cyt*C* (7 µM), NADPH (3 mM) and FldR (0.17 µM) were mixed together, and absorption spectra were measured after 0, 90, 180, 270 and 360 seconds.

2.5.3. Testing of the ability of the FldRs to reduce flavodoxins from *B. cereus*

FMN absorbs light at 460 nm in its oxidised form. The absorption peak at this wavelength is decreased when FMN is in the sq (partially reduced) form, and a new peak appears at 600 nm. When the cofactor is in the hq (fully reduced) form, both these peaks have disappeared [Berg, Tymoczko and Stryer, 2007]. These properties of the FMN cofactor were used to monitor the reduction of NrdI.

The ability of the FldRs to reduce the flavodoxin-like protein NrdI from *B. cereus* was tested in the following manner. (The NrdI was previously purified in our group.)

1) Tris·HCl buffer (100 mM; pH 7.5) and NrdI (10 µM) was mixed together in a cuvette and made anaerobic with a Schlenk line, before the first absorption spectrum was measured.

2) NADPH (100 μM) was made anaerobic and added to the mixture, before the second absorption spectrum was measured.
3) FldR (1.6 μM) was added to the mixture, and absorption spectra was measured after 20 seconds and 30 minutes.

3. Results and discussion

3.1. Cloning of *BC0385* into the pET-22b expression vector and generation of FldR BC0385 expressing *E. coli* cells

To generate and amplify *BC0385* gene fragments for later cloning into a pET-22b vector, PCR was performed with primers designed with NdeI and HindIII restriction sites and *B. cereus* genomic DNA as template. The PCR mixtures from each of the wells in the temperature gradient (**Table A2.1**) were tested and purified with agarose gel electrophoresis (**Figure 3.1.1**). The picture of the gel taken with an ultraviolet light-camera showed that all annealing temperatures tested turned out to give a similar amount of PCR product. It was therefore not possible to determine which of the temperatures in the selected range that was the most optimal. However, measurement of the DNA concentrations in the respective reactions after purification from the agarose gel indicated that the PCR with annealing temperatures 57.6 °C and 66.3 °C were the ones with the highest concentrations; 57.1 ng/µL and 60.8 ng/ µL, respectively. It can be derived from this that these two temperatures were the most effective for the primers that were designed and used (section A5.3). Therefore, these two samples of *BC0385* were chosen for further work.

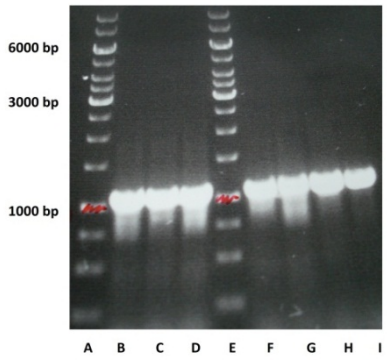

Figure 3.1.1: PCR mixtures in agarose gel after reaction and separation by electrophoresis. A + E) DNA standard (Figure A1.1), B-D + F-I) PCR mixtures with annealing temperatures increasing from left to right.

The pET-22b vector was amplified by growing cells containing this plasmid, and thereafter purified from the cell culture. Initial attempts resulted in concentrations too low for a successful cloning experiment with *BC0385*. The ligation protocol from the manufacturer [Fermentas Inc, 2011] of the T4 DNA ligase and the ligase buffer recommends 20-100 ng of vector DNA (and insert DNA in a 1:1 to 5:1 molar ratio over vector). Additional attempts where the NucleoSpin-protocol was slightly modified (see section A.6.1.), however, resulted in satisfying vector concentrations; 70.3 ng/µL and 67.0 ng/µL.

Samples of *BC0385* and pET-22b were separately digested with NdeI and HindIII restriction enzymes, and ligated with *BC0385* in a 3:1 molar ratio over vector. Competent *E. coli* cells were transformed with the ligation product and spread onto agar plates. Observation of cell colonies after incubation over night indicated successful transformation. Initial transformation attempts by the use of chemocompentent *E.coli* cells (made by Inger Olsbu in our lab) gave no colonies. Neither did the attempt using the commercial *E. coli* BL21 (DE3) Competent cells (BL21-cells). However, further transformation attempts, using the commercial competent *E. coli* XL10-Gold ultracompentent cells (XL10-cells) gave more than 30 colonies on each agar plate. The XL10-cells are designed for an effective uptake of large plasmids, while the BL21-cells are designed for effective protein expression. Apparently, the concentration of plasmid in the sample was too low for the BL21-cells to take it up. The negative results with the non-commercial chemocompetent *E. coli* cells, on the other hand, may have several explanations; the cells might have been stored improperly, errors might have occurred during the procedure of making the cells chemocompetent, or the transformation protocol may be unsuitable for these cells, to mention some.

Plasmid was purified in 20 parallels from cell cultures made from 20 single colonies, respectively. A small sample from each parallel was cut with the same restriction enzymes as earlier and analysed by agarose gel electrophoresis. This was to test if *BC0385* was inserted in the vector. The testing did not indicate a successful insertion for any of the colonies that were picked. Therefore, modifications were made to the process of restriction cutting; the restriction enzymes and buffer used in the first trial were replaced with FastDigest enzymes and buffer (from Fermentas, like those previously used). After the transformation of XL10-cells a very weak band of~1000 base pairs was visible, in addition to a band of~5500 base pairs, for 1 of the 20 investigated colonies (**Figure 3.1.2**).

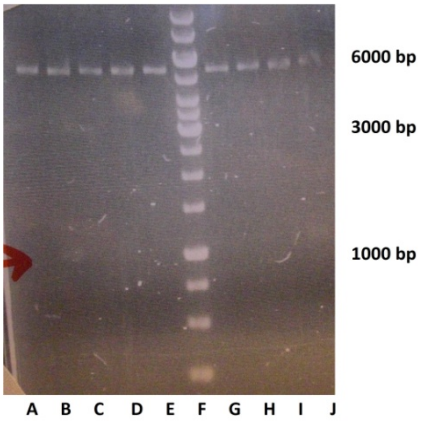

Figure 3.1.2: Digestion products after test cutting in agarose gel after separation by electrophoresis. A-E + G-I) digestion products from 9 of the 20 investigated colonies, F) DNA standard. In lane B there is a barely visible band of around 1000 base pairs (indicated by the red arrow) in addition to the band of around 5500 base pairs, indicating that this sample may contain a plasmid with the gene inserted.

The sequencing of the plasmid confirmed that *BC0385* was successfully cloned into the pET-22b vector, but it also uncovered a C114A point mutation. This point mutation was a so-called *missense mutation*, i.e. it would have led to an amino acid substitution in the protein sequence if translated. That is because the codon made up of base pairs 112-114 is originally CAC, which codes for histidine, whereas the mutated codon, CAA, codes for glutamine. Therefore, primers with an A114C point mutation were designed, followed by PCR with these primers and the pET-22b vector with the mutated insert as template. XL10-cells were transformed with the PCR product from each of the 4 different annealing temperatures used. The number of colonies on the agar plates after incubation over night was decreasing (from 50 colonies to 7 colonies) with increasing annealing temperature. This indicates that the primers had a relatively low melting temperature. Single colonies from the plate with the highest number of colonies were cultured, and the plasmid was sequenced after purification. The normal T7 primer was used in three parallels and T7 terminator primer in three additional parallels. The use of T7 terminator primer allowed determination of the last part of the gene sequence with higher precision, as the chromatograms from the use of T7 primer could not give usable information for this part of the sequence. The result showed that the mutagenesis had been successful, and that the codon now was CAC as in the native gene.

BL21-cells were successfully transformed with the plasmid. An expression test was performed before the cells were grown in high amounts, in parallel with a culture to which IPTG was not added (as a negative control) and cells expressing the other FldR as a control (**Figure 3.1.3**). The expression test indicated that *E. coli* cells expressing FldR BC0385 (38.7

kDa) had been successfully generated, because a protein of ~38 kDa was indicated to be overexpressed in the system. However, the protein seemed to be highly expressed even when the inducer, IPTG, was absent (**Figure 3.1.3**). This was confirmed by several expression tests. The manufacturer of the BL21-cells states that T7 RNA polymerase is expressed from a promoter which is less sensitive to catabolite repression than the wild type promoter, and that this can lead to uninduced target protein expression [New England Biolabs, 2012].

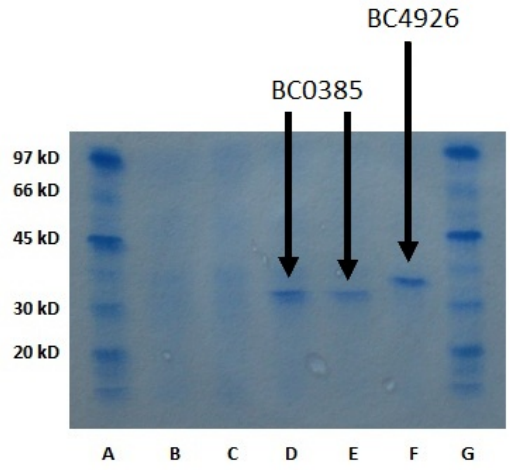

Figure 3.1.3: Expression of FldR BC0385 and FldR BC4926. A) Protein standard; B) BC0385 before induction; C) BC4926 before induction; D) BC0385 after 15 hours growth; E) BC0385 after induction and 15 hours growth; F) BC4926 after induction and 15 hours growth; G) Protein standard.

3.2. Expression and purification of FldR BC0385 and FldR BC4926

FldRs BC0385 and BC4926 were both over expressed in the presence of IPTG, and purified for later protein crystallisation, crystal structure determination and activity measurements. Both proteins were treated approximately equally, using the same expression procedures, purification procedures, growth media, buffers and solutions.

After cell lysis, initial removal of cell matter and precipitation of DNA, the protein was precipitated (*salted out*) by the addition of $(NH_4)_2SO_4$. The minimal concentration of $(NH_4)_2SO_4$ needed to salt out all FldR BC4926 from solution had already been optimised to 0.22 g/mL. With respect to the FldR BC0385, the required amount of $(NH_4)_2(SO)_4$ was not investigated because of time limitations; 0.43 g/mL was chosen as a starting point.

3.2.1. Purification of FldR BC0385

After desalting chromatography, anion exchange chromatography was performed. In the case of FldR BC0385 (**Figure 3.2.1 A**) there was a relatively high amount of other proteins in the sample. This could possibly be explained by that the amount of $(NH_4)_2SO_4$ needed to salt out the protein was not optimised, and illustrates the benefit of optimising this purification step (when compared to FldR BC4926 where this was optimised, see **Figure 3.2.2 A**). If the required amount is lower than 0.43 g/mL, it will be possible to obtain a sample with a lower amount of other proteins before the chromatography steps. Especially if the proteins that were eluted at a conductivity similar or close to that of FldR BC0385 had higher solubility than FldR BC0385, then the optimisation of the $(NH_4)_2SO_4$ precipitation would have resulted in a purer sample of FldR. In addition, since the chromatography columns have a limited protein capacity, a purer protein sample would increase the amount of sample that can be purified per turn. The protein was eluted at 35 mS/cm (26 % buffer C), as seen by the overlap of a 280 nm peak with a 450 nm peak (the flavin cofactors FAD and FMN both absorbs light at 450 nm). The initial runs showed that pH 7.5 appeared to be too low for the FldR to have enough negative charge to bind significantly to the column. Therefore, the pH was increased to 8.1, which appeared to be efficient. The upper value of the salt gradient, 40 %, and the length of it, 190 mL, was chosen as starting points, and turned out to give an acceptable separation of the FldR from the other proteins. During the first runs, where also the salt gradient was tried optimised, a physical error (leakage) occurred in the Äkta purifier system and hence the purification and optimisation could not continue. However, a small amount of FldR BC0385 had been collected and further purified by gel filtration chromatography before this error occured. The gel filtration chromatogram shows that the protein became considerably purer after this step, although the FldR BC0385 gel filtration peak is not completely separated from a smaller peak upstream (**Figure 3.2.1 B**).

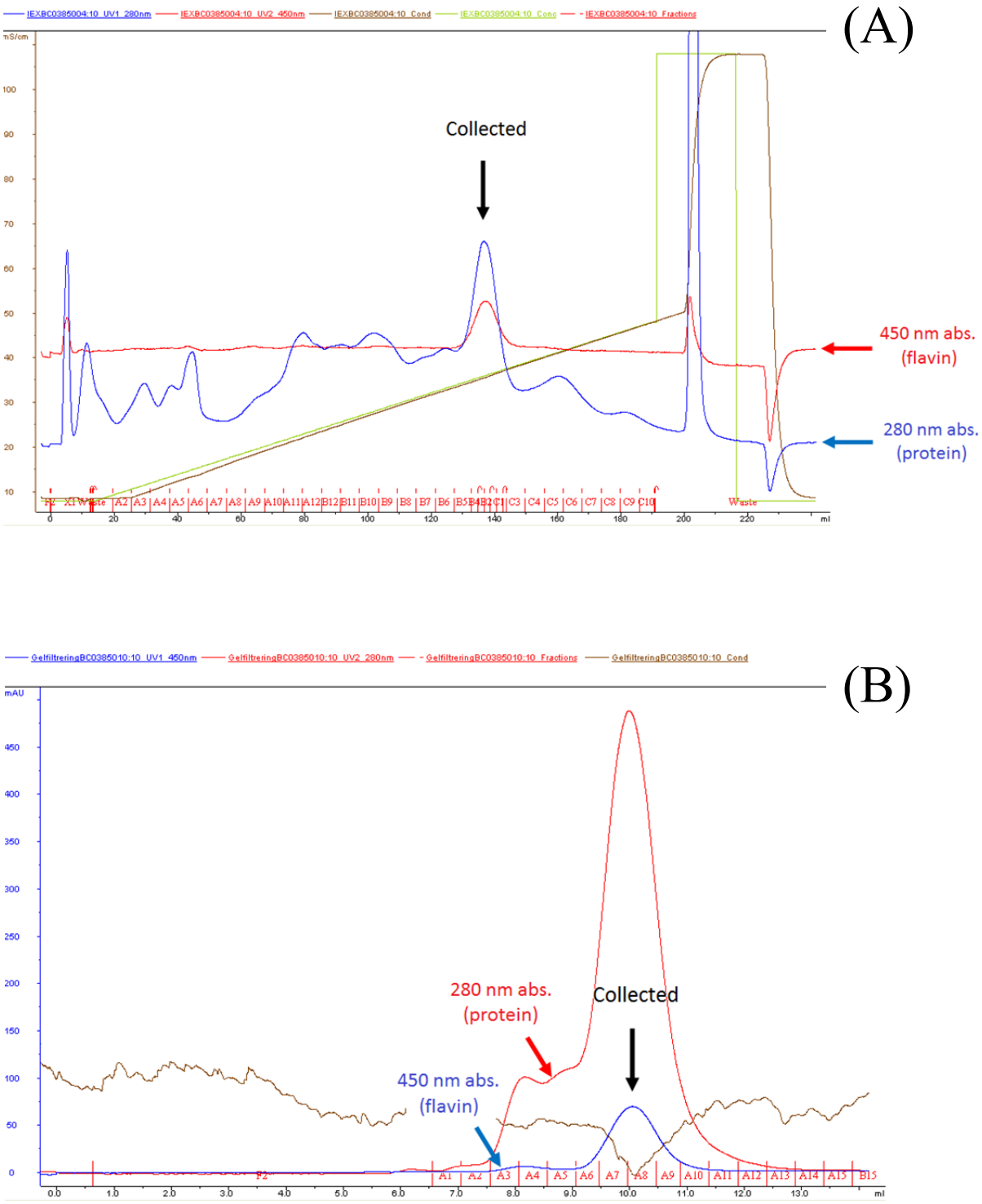

Figure 3.2.1: Chromatograms from the purification of FldR BC0385. The absorbances at 280 nm and 450 nm were recorded as a function of mL eluent and are indicated by the blue and the red line. A) Chromatogram fro anion exchange. The protein was eluted with buffer B and an increasing amount of buffer C (high salt; green line). The conductivity is indicated by the brown line and was also recorded as a function of ml eluent. Fractions under the 450 nm absorption peak in the range of 132-142 mL were collected. B) Chromatogram from gel filtration. The protein was eluted with buffer D. Fractions under the 450 nm absorption peak in the range of 9.5-11.0 mL were collected.

3.2.2. Purification of FldR BC4926

In the case of FldR BC4926 there was a relatively low amount of other proteins in the sample when it was run through the anion exchange column, presumably due to the low amount of $(NH_4)_2SO_4$ needed to salt out the protein from solution (**Figure 3.2.2 B**). The $(NH_4)_2SO_4$ precipitation was therefore a successful purification step. Initial runs showed that pH 7.5 was too low for FldR BC4926 to bind effectively to the anion exchange column. The pH in the protein sample and the buffers was therefore increased in small steps, and at pH 8.1 the protein had enough negative charge to bind effectively to the column. The salt gradient was optimised, with regard to both the target concentration of buffer C (high salt content) and the length of the gradient; see **Figure 3.2.2** for chromatograms before and after optimisation, respectively. The target concentration of buffer C was optimised to 25 %, which equals 33 mS/cm, and it was observed that the protein comes in two forms, one apo form and one flavo form – this was confirmed with SDS-PAGE. The apo-FldR was eluted at approximately 20 mS/cm and the flavo-FldR at a slightly higher conductivity. The length of the gradient was optimised to be 145 mL, which showed to give an acceptable separation of apo-FldR and flavo-FldR.

After the development of a standard purification protocol for FldR BC4926, the total yield of protein obtained from the purification process should have been estimated. However, due to an error in the Äkta purification system leading to a leakage of an unknown amount of protein from the system, a correct yield could not be estimated.

Because of efficiently higher yield of apo-FldR than of flavo-FldR, reconstitution of flavo protein from apo-FldR and flavin was tried. For this, an initial experiment was needed to investigate which one of the two flavin candidates that is utilised by the protein. In two parallels, FAD and FMN were added to a sample of apo-FldR and purified on a desalting column. The results indicate that FAD is the right cofactor for FldR BC4926 (**Figure 3.2.3**). In this case, there was an overlap of the 280 nm absorption peak with a 450 nm absorption peak, which for the FMN case was barely visible. The flavin cofactors absorb some light at 280 nm in addition to at 450 nm, which is the reason for the relatively higher “protein peak” (280 nm absorption) in the FAD case compared to the FMN case.

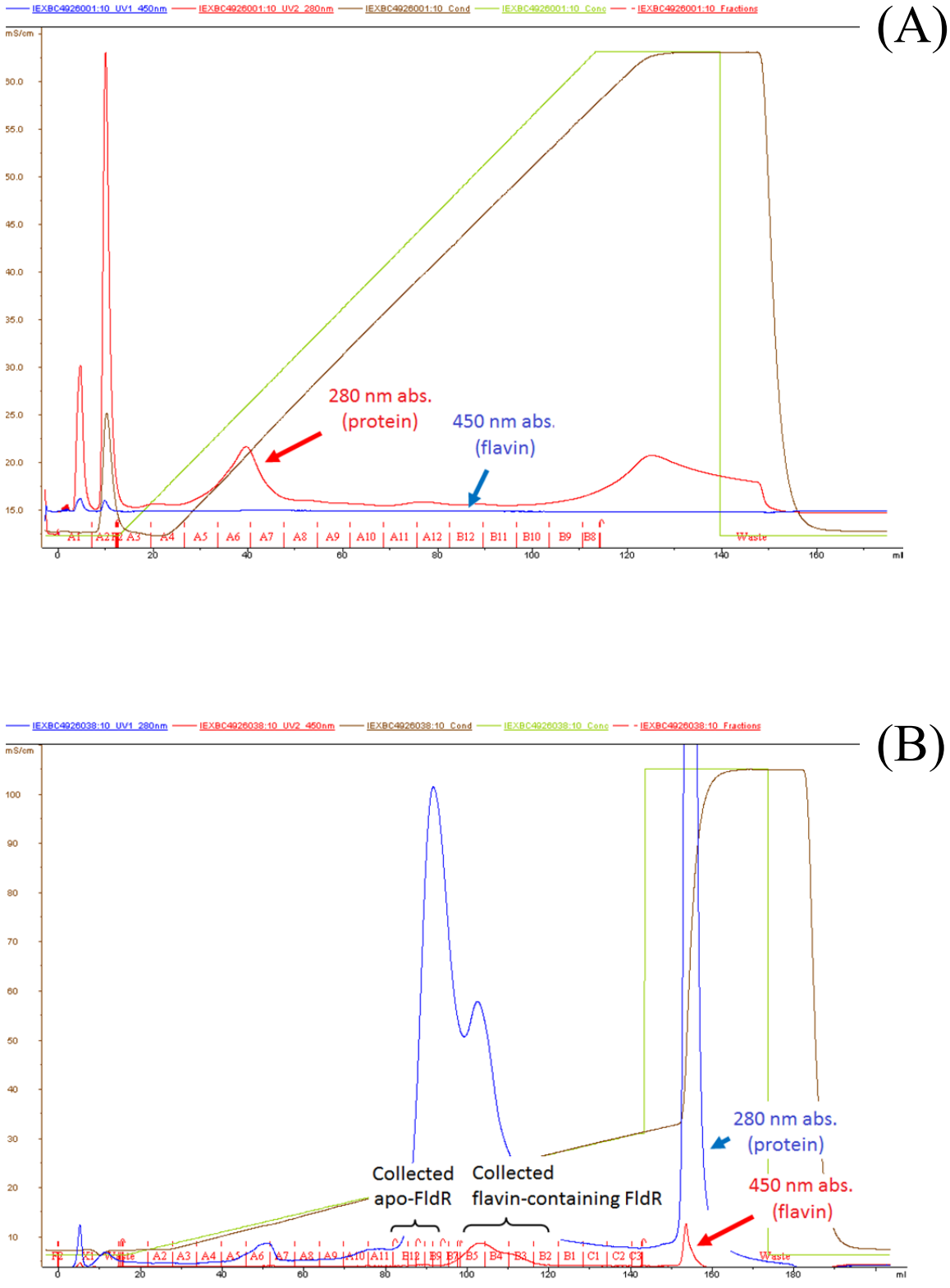

Figure 3.2.2: Chromatogram from anion exchange chromatography of FldR BC4926. A) Before optimisation of the pH and the salt gradient. B) After optimisation.The protein was eluted with buffer B and an increasing amount of buffer C (high salt). The conductivity is indicated by the green line and was also recorded as a function of ml eluent. Fractions under the highest 280 nm absorption peak in the range of 85-95 mL were collected for the apo-FldR, whereas fractions under the 450 nm peak in the range of 100-115 mL were collected for the flavin-containing FldR.

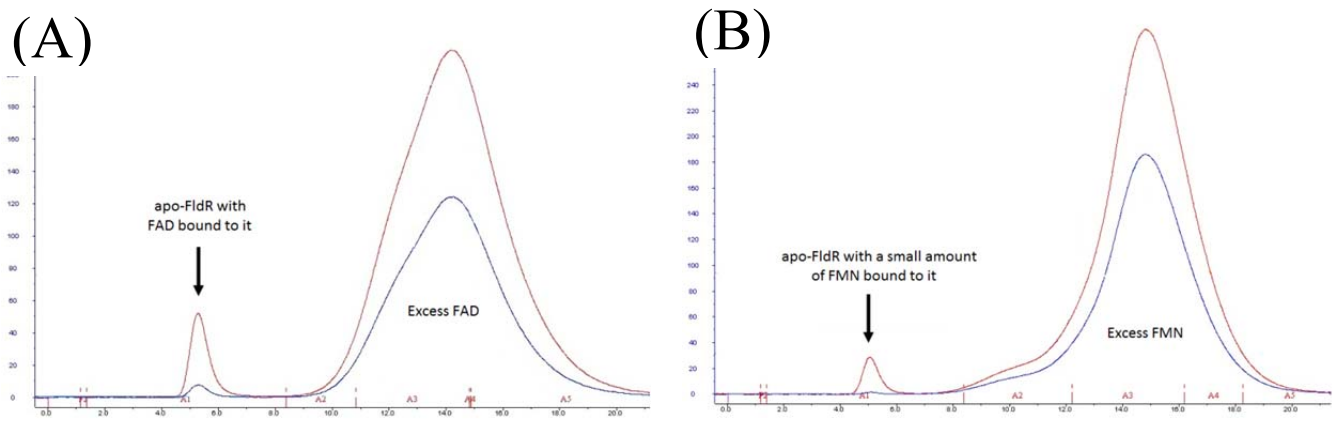

Figure 3.2.3: Chromatograms from size exclusion chromatography (by use of a desalting column) of apo protein samples with added FAD (A) and FMN (B). The absorbances at 280 nm and 450 nm was recorded as a function of mL eluent and are indicated by the red and the blue line, respectively. In the case of FAD there is a 450 nm absorption peak which overlaps with the 280 nm absorption peak, indicating that this is the right cofactor.

Higher amounts of reconstituted protein were purified by gel filtration chromatography (**Figure 3.2.4**). The chromatogram shows that the protein purity increases, however, it was not possible to collect protein fractions without contamination from a peak upstream.

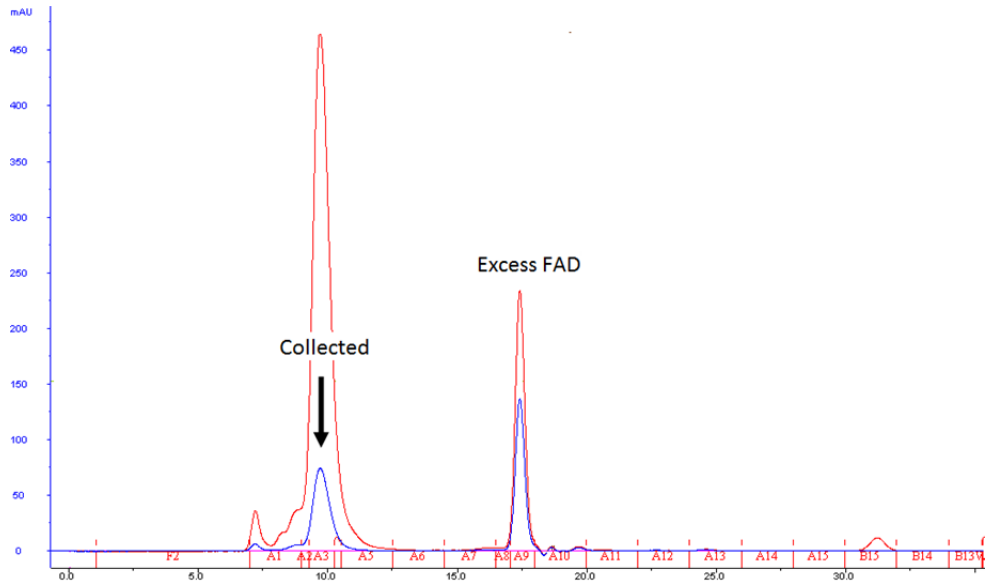

Figure 3.2.4: Chromatogram from gel filtration of reconstituteed flavo protein. Fractions under the 450 nm absorption peak in the range of 9.0-10.5 mL were collected. The absorbances at 280 nm and 450 nm were recorded as a function of mL eluent and are indicated by the red and the blue line, respectively.

The reconstituted, purified protein did precipitat at a concentration of approximately 2 mg/mL, and during up-concentration, it was observed that FAD was gradually released from the protein. Screening for crystallisation conditions with the reconstituted FldR gave no hits. This led to increased work on the apo-FldR instead, since the yield of this form was relatively high. The apo-FldR was therefore purified by gel filtration chromatography and the chromatogram shows that the apo protein was highly pure after this step (**Figure 3.2.5 A**).

In addition, native flavo-FldR BC4926 was purified by gel filtration chromatography and the chromatogram shows that this protein was successfully purified from other proteins (**Figure 3.2.5 B**). From visual inspection of the sample, it was indicated that the native flavo-FldR BC4926 was of a much higher concentration than the reconstituted one, because of the higher density of yellow colour (which is caused by the oxidised flavin). When comparing **Figure 3.2.1** and **Figure 3.2.5 B**, however, it is observed that the flavin-to-protein ratio is higher in the case of FldR BC0385 than in the case of native flavo-FldR BC4926. When looking at the chromatogram from ion exchange chromatography with the latter protein (**Figure 3.2.2 B**), the different flavin-to-protein ratios can be explained by the fact that the apo-FldR peak to a large extent overlaps with the flavo-FldR peak. Hence, after gel filtration chromatography, the sample of native flavo-FldR contains an unknown amount of apo-FldR, lowering the flavin-to-protein ratio in the flavo-FldR sample. If the flavo-FldR BC4926 is more stable at higher concentrations with apo-FldR present in the solution, this could be a possible explanation to the observation that the reconstituted protein appears to behave differently from the native one.

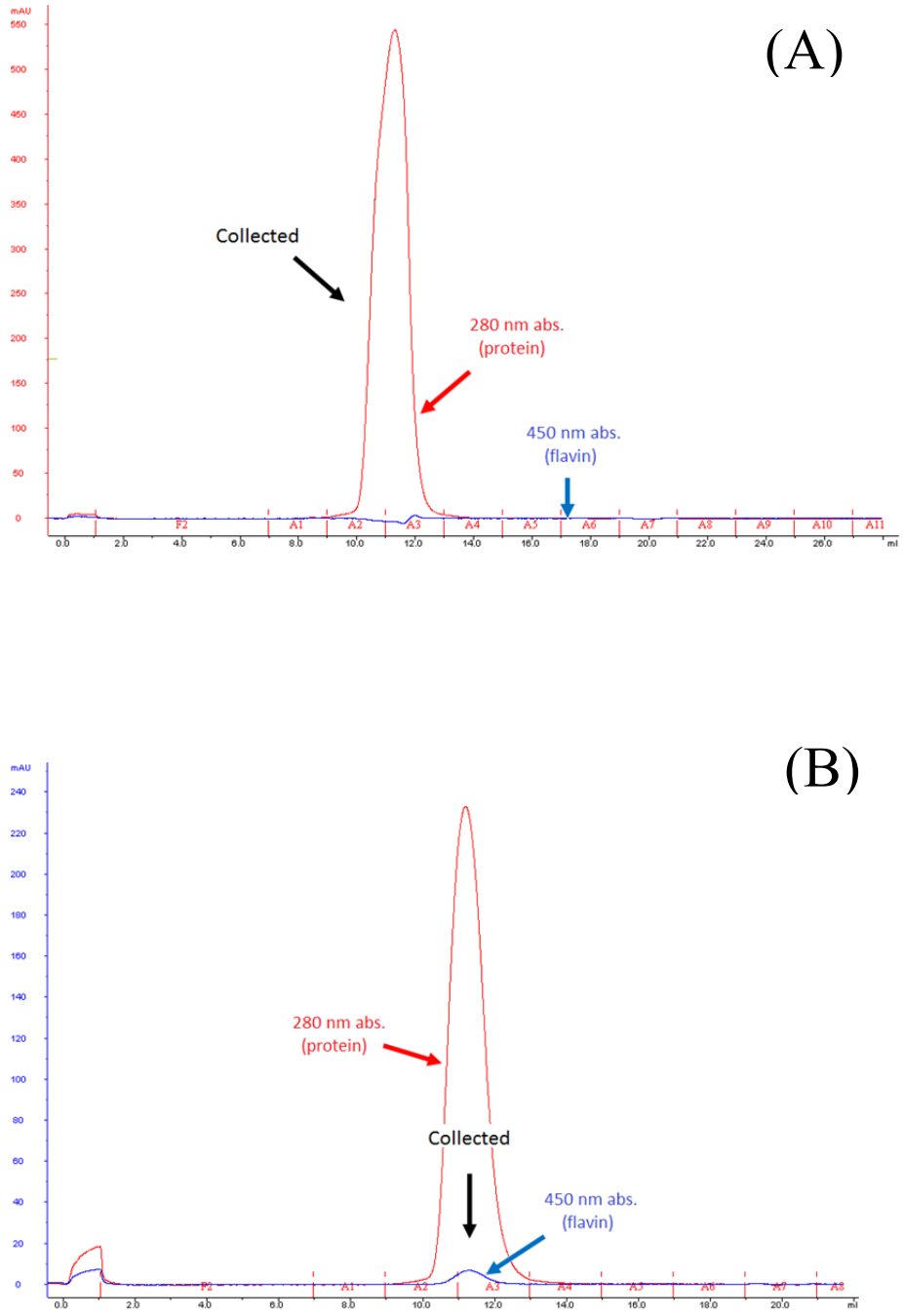

Figure 3.2.5: A) Chromatogram from gel filtration of apo protein. Fractions under the 450 nm absorption peak in the range of 9.5-12.5 mL were collected. B) Chromatogram from gel filtration of native flavo protein. Fractions under the 450 nm absorption peak in the range of 9.0-13.0 mL were collected. The absorbances at 280 nm and 450 nm were recorded as a function of mL eluent and are indicated by the red and the blue line, respectively.

3.3. Protein crystallisation and X-ray diffraction

The results from the screening experiments with the different FldRs are summarised and presented in **Table 3.3.1**. The results and attempts of optimising the conditions that gave hits are described in more detail below.

Table 3.3.1: Summary of the screening experiments with the different FldRs

Protein	Screens	Hits
FldR BC0385	JCSG+ and Index	Index, H12 (cubes and needles)
FldR BC4926, reconstituted	JCSG+, Natrix (E-H) and PEG/Ion (A-D) and Wizard I+II	None
apo-FldR BC4926 (~15 mg/mL)	JCSG+, PEG/Ion and Wizard I+II	None
apo-FldR BC4926 (~60 mg/mL conc.)	JCSG+ and Midas	JCSG+, H11 and H12 (needles)
FldR BC4926	Index, JSCG+ and Wizard I+II	Index, F2; JCSG+, A7 and B3

3.3.1. Crystallisation of FldR BC0385

After gel filtration chromatography, the protein sample was concentrated up to the point where it almost started to precipitate. In the screening for crystallisation conditions for this FldR, only two commercial screens were tried out because of limited amounts of protein. For the Index screen, the condition in well H12 gave a positive result in the most concentrated drop (**Figure 3.3.1**); 1 cubic shaped protein crystal of approximately 0.03 mm x 0.03 mm x 0.02 mm together with 5-8 smaller cubes and some thin needles.

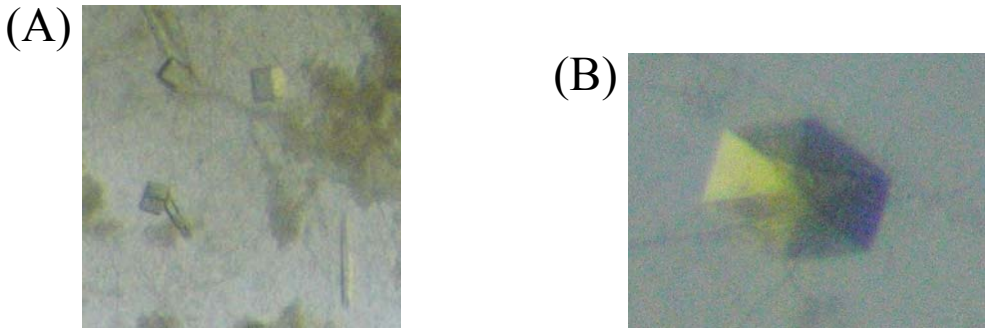

Figure 3.3.1: Crystals of FldR BC0385. A) The condition in well H12 of the Index screen favoured both cubic shaped crystals and needle shaped crystals. B) Close up photo of the largest crystal (0.03 mm x 0.03 mm x 0.02 mm), which were subject for an x-ray diffraction experiment.

3.3.2. X-ray diffraction experiment on the FldR BC0385 crystal

The FldR BC0385 crystals diffracted to ~7-8 Å as seen by the diffraction image in **Figure 3.3.2**, where the resolution at the edge of the Pilatus 6M Dectris detector was 2.5 Å. The diffraction images were collected at ID29 at ESRF with a flux of $1.4 \cdot 10^{12}$ photons/sec (100 % transmission), exposure time 0.1 second and oscillation range 1.0°. Increased exposure time did not increase the diffraction limit. Therefore, no complete data sets were collected on the crystals.

The unit cell was determined with MOSFLM to be a=94.7 Å, b=101.4 Å, c= 114.2 Å, α=90°, β=94.9°, γ=90°, based on a good fit with the diffraction spots, and giving a low penalty. The crystal system was confirmed with POINTLESS to be monoclinic.

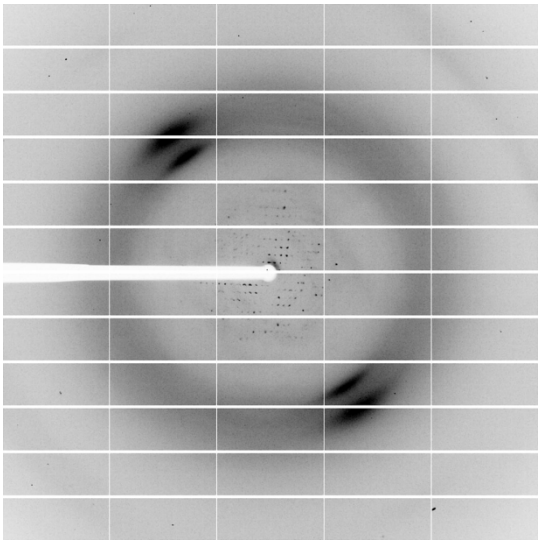

Figure 3.3.2: Example of a diffraction image from the initial diffraction experiment with the BC0385 crystals. It can be seen that the crystals diffracted poorly because of the low amount of spots.

3.3.3. Crystallisation of FldR BC4926

After gel filtration chromatography, the sample of reconstituted FldR BC4926 was concentrated up to the point where it almost started to precipitate; approximately 2 mg/mL. In the screening for crystallisation conditions for this FldR, six commercial screens were tried out with no positive results (**Table 3.3.1**).

After gel filtration chromatography, the sample of apo protein was concentrated to ~15 mg/mL in one screening experiment and to~60 mg/mL in a separate screening experiment. For the second experiment, the conditions in wells H10 and H11 for the JSCG+ screen gave positive results in the form of needles. The attempts of optimising these conditions with regard to their protein and PEG contents resulted in slightly thicker needles for the H10 condition with 25 % PEG (**Figure 3.3.3**).

Figure 3.3.3: Crystals of FldR BC4926 apo form. The conditions in wells H10 and H11 of the JSCG+ screen both favoured needles, with slightly thicker needles for H10 with a lowered PEG content (pictured).

Only negative results for the reconstituted FldR BC4926 encouraged focusing on the native flavo-FldR, despite the low yield. After gel filtration chromatography, the sample was concentrated up to the point where it almost started to precipitate. Screening with the native flavo-FldR BC4926 gave hits in wells A7 and B3 for the JSCG+ screen and in well F2 for the Index screen, all in the form of needles (**Figure 3.3.4.**).

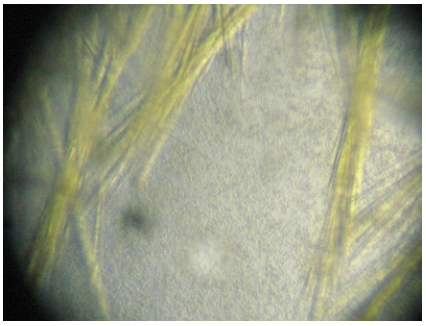

Figure 3.3.4: Crystals of FldR BC4926 flavo form. The conditions in wells A70 and B3 of the JSCG+ screen and F2 of the Index screen all favoured needles like this.

Chemicals were available for the JSCG+ conditions, and these were tried optimised regarding their protein and PEG contents. The A7 condition gave slightly thicker needles for some of the new conditions that were set up. Therefore, sitting drop experiments of higher volumes as

well as some hanging drops were set up with these conditions. An improvised seeding experiment was also performed. All this resulted in needles of the approximate same size as the ones that were obtained initially.

3.3.4. X-ray diffraction experiment on FldR BC4926 crystals

The apo-FldR BC4926 needle crystals diffracted very poorly to only 10-15 Å at X10SA with 100 % transmission. As the native flavo-FldR BC4926 crystals were of the same size and shape as those of the apo-FldR, no diffraction experiments were performed with them. Du to time limitation no further crystallisation attempts were made to give better crystals of this FldR.

3.4. Activity measurements

3.4.1. Determination of the specific activity of the FldRs with DCPIP

The activities of the FldRs were compared by determination of the K_m value of each FldR with NADH as the electron donor and DCPIP as the electron acceptor. The molar reduction of DCPIP was measured by following the drop in absorption at 600 nm (ΔA_{600}), illustrated in **Figure 3.4.1**.

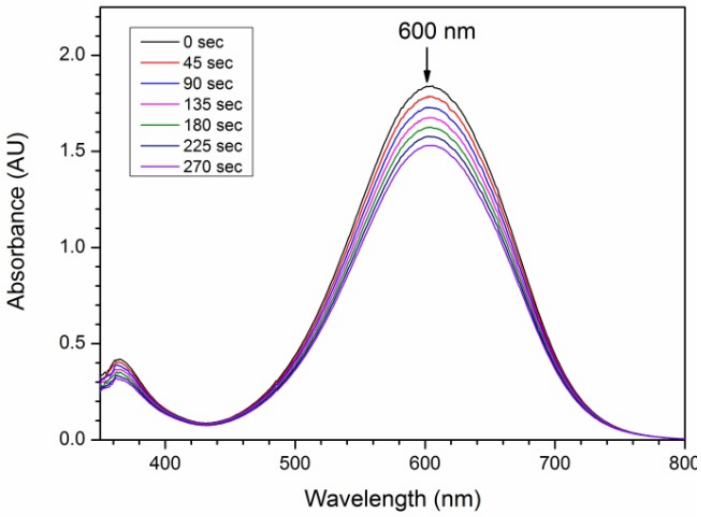

Figure 3.4.1: NADH, FldR and DCPIP mixed together leads to a drop in the absorbance at 600 nm over time. This illustrates the reduction of DCPIP, which is catalysed by FldR. The illustration of the principle is representative for both FldRs.

The absorption was measured every 15 seconds for 240 seconds in total, and the reaction turned out to be linear during the whole time interval for both FldRs. Therefore, ΔA_{600} between 0 and 240 seconds was used as the basics for the calculations. The amount of reduced DCPIP after 240 seconds in each reaction was determined with $\varepsilon_{600} = 20.6\ cm^{-1}\ mM^{-1}$ [Armstrong, 1964] and plotted against the respective concentration of DCPIP. Thereafter, a Michaelis-Menten curve fit was estimated for the plot using Origin. The results are presented in **Figure 3.4.2** and **Figure 3.4.3**. Measurements with DCPIP concentrations above 400 µM showed a lower V_0 than for 270 µM DCPIP. When they were included in the plot, the fitted curve followed the typical features of substrate inhibition [Palmer, 1991]. When the measurements with concentrations above 400 µM were excluded, K_m was estimated by the program to be 405 µM for FldR BC0385.

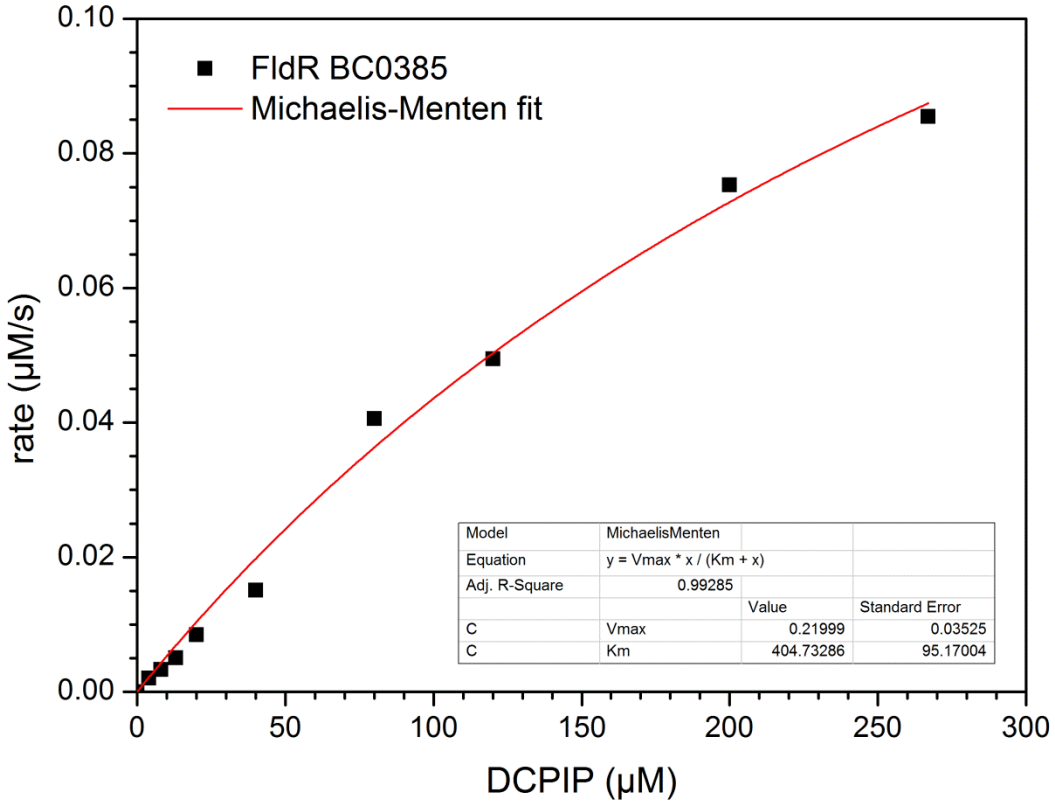

Figure 3.4.2: Plot of the different reactions using FldR BC0385 as the catalyst (black, cubic spots). The red line indicates the fitted Michaelis-Menten curve which was estimated in Origin. The estimated K_m value of this enzyme was 404 µM.

In the case of FldR BC4926, the K_m was estimated to be 1.5 µM, indicating that this FldR is 200-fold more effective than FldR BC0385 when DCPIP is the substrate. Because DCPIP is reduced by two electrons [Dupuy, 2004], this indicates that FldR BC4926 is a more effective two-electron donor than FldR BC0385 is.

The presented results are only based on one parallel, because of limitations with regard to both time and protein. This means that they have to be considered as initial results, and further measurements have to be performed for the activities to be determined with a higher degree of accuracy.

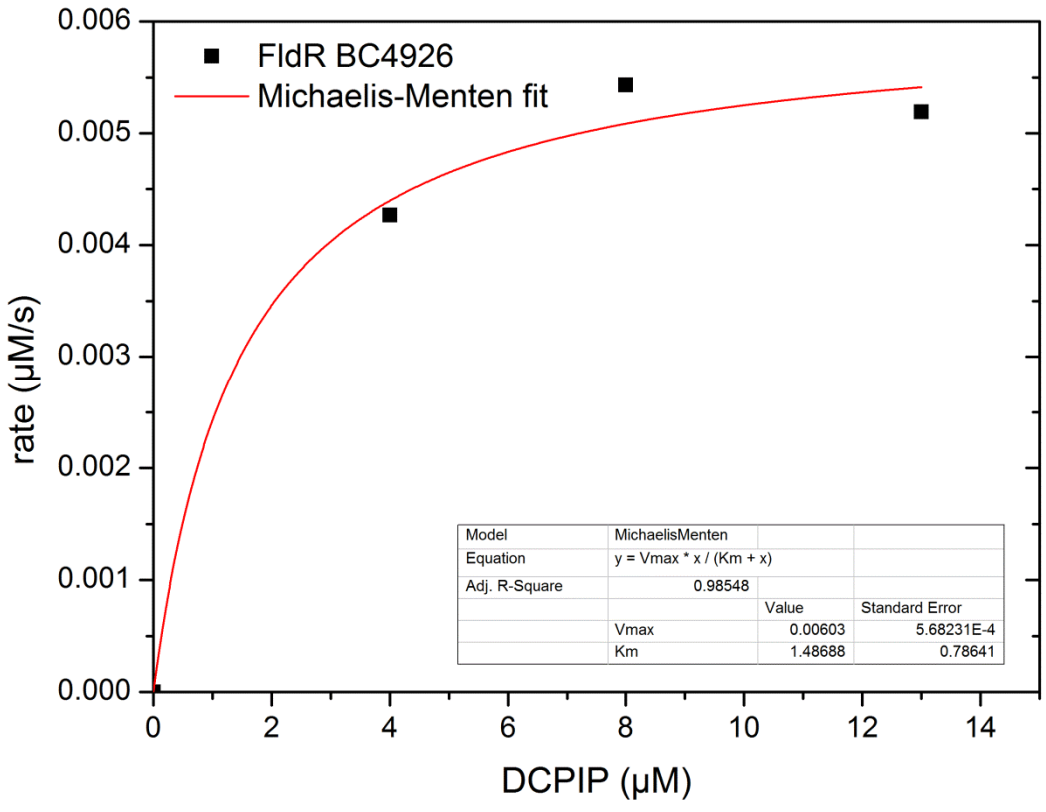

Figure 3.4.3: Plot of the different reactions using FldR BC4926 as the catalyst (black, cubic spots). The red line indicates the fitted Michaelis-Menten curve which was estimated in Origin. The estimated K_m value of this enzyme was~1.5 µM.

3.4.2. Comparison of the FldR activities with cytochrome *c*

The ability of the FldRs to reduce Cyt*c* was compared by monitoring the reduction of the 550 nm Cyt*c* absorption peak over a time period of 360 seconds. The result is presented in **Figure 3.4.4**, showing that FldR BC0385 reduces CytC more effectively than FldR BC4926 does. As Cyt*c* is reduced by one electron only [Krab and Wikström, 1979], the results indicates that BC035 is more effective in one-electron donation than FldR BC4926 is.

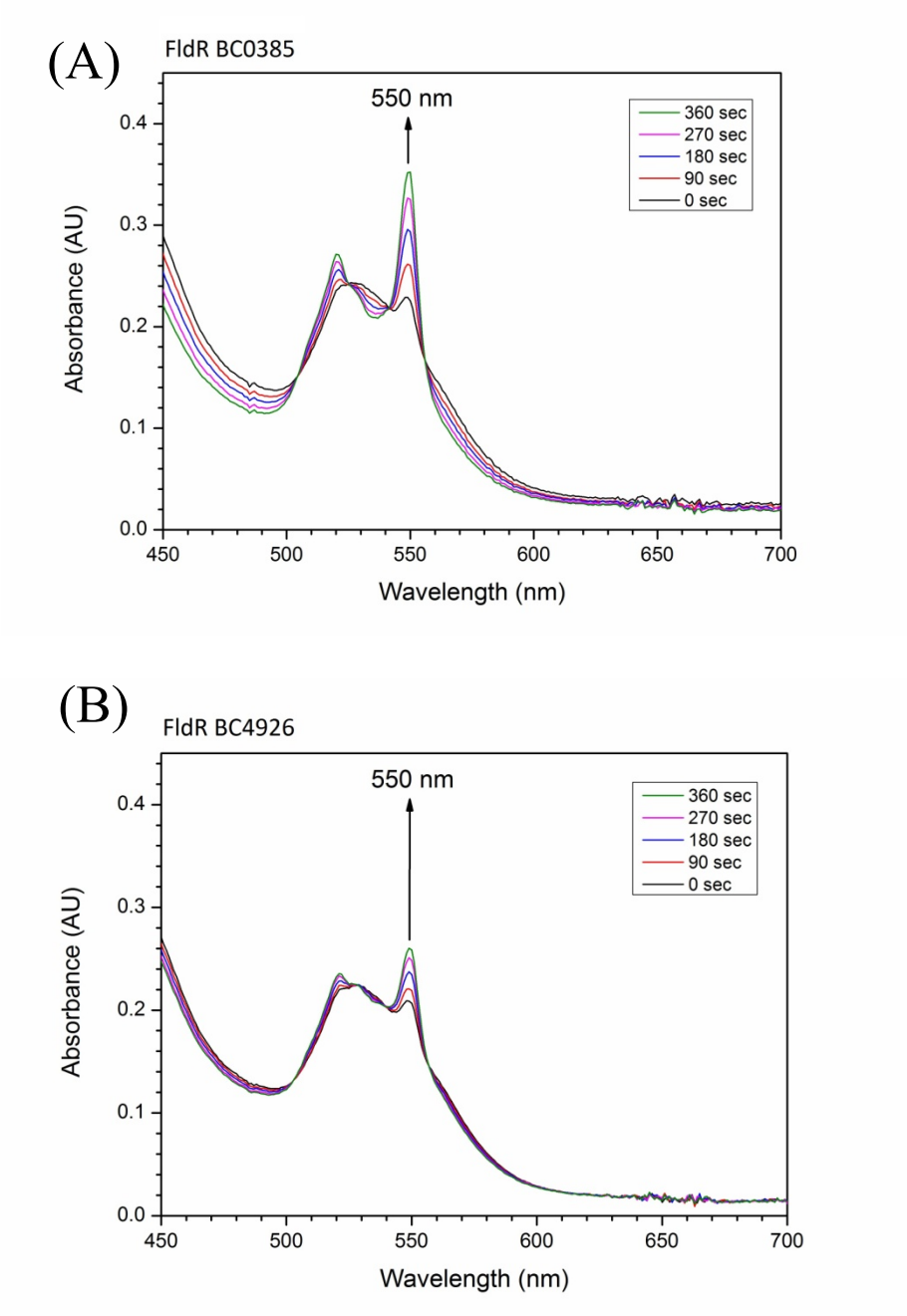

Figure 3.4.4: NADPH, FldR and Cyt*c* mixed together leads to an increase in the absorbance at 550 nm over time. This illustrates the reduction of Cyt*c*, which is catalysed by FldR. It is absorbed a higher degree of increase in the case of FldR BC0385 (A) than in the case of FldR BC4926 (B).

3.4.3. Testing of the ability of the FldRs to reduce flavodoxins from *B. cereus*

To obtain some information about possible redox partners of the two FldRs *in vivo*, the ability to reduce the flavodoxin-like NrdI from *B. cereus* was tested for each of them. The results were compared with the ability of the FldRs to reduce Fld BC1376 and Fld BC3541. These proteins are also encoded by *B. cereus*, and were studied by Marie Lofstad in our group. The ability of the FldRs to reduce these flavodoxins was performed by her with the same concentrations and conditions as the experiments with NrdI.

As seen from **Figure 3.4.4** and **Figure 3.4.5**, the pair FldR BC4926 and Fld BC3541 (FLD2) results in the most effective transfer of electrons (**Figure 3.4.4d**), followed by the pair FldR BC4926 and Fld BC1376 (FLD1) (**Figure 3.4.4c**). In these cases, reduction of the FMN cofactor is clearly seen by the decrease of the 340 nm peak and the appearance of a peak at 600 nm, which is characteristic for the sq (partially reduced) form. NrdI does not appear to be significantly reduced by any of the FldRs (**Figure 3.4.5**), because the peak at 460 nm, characteristic for the oxidised form of FMN (the cofactor of NrdI) remains constant, both after 20 seconds and 30 minutes. The absorption at 340 nm is characteristic for reduced NADPH, and the drop indicates electron transfer. However, no reduction of the FMN is indicated after 20 seconds or 30 minutes, and therefore the oxidation of NADPH probably arise from that electrons flow from NADPH via FldR to O_2 (from system leakage). On the other hand, the oxidation of NADPH in the case of the pair FldR BC0385 and Fld BC1376 (FLD1) (**Figure 3.4.4a**) is much slower than in either of the experiments with NrdI. Therefore, it can not be excluded that (rapid) re-oxidation of FMN from O_2 (leakage) explains the apparent lack of correspondence between NADPH oxidation and FMN reduction. However, these measurements need to be repeated under more controlled anaerobic conditions, and in the exact same way to avoid different systematic errors.

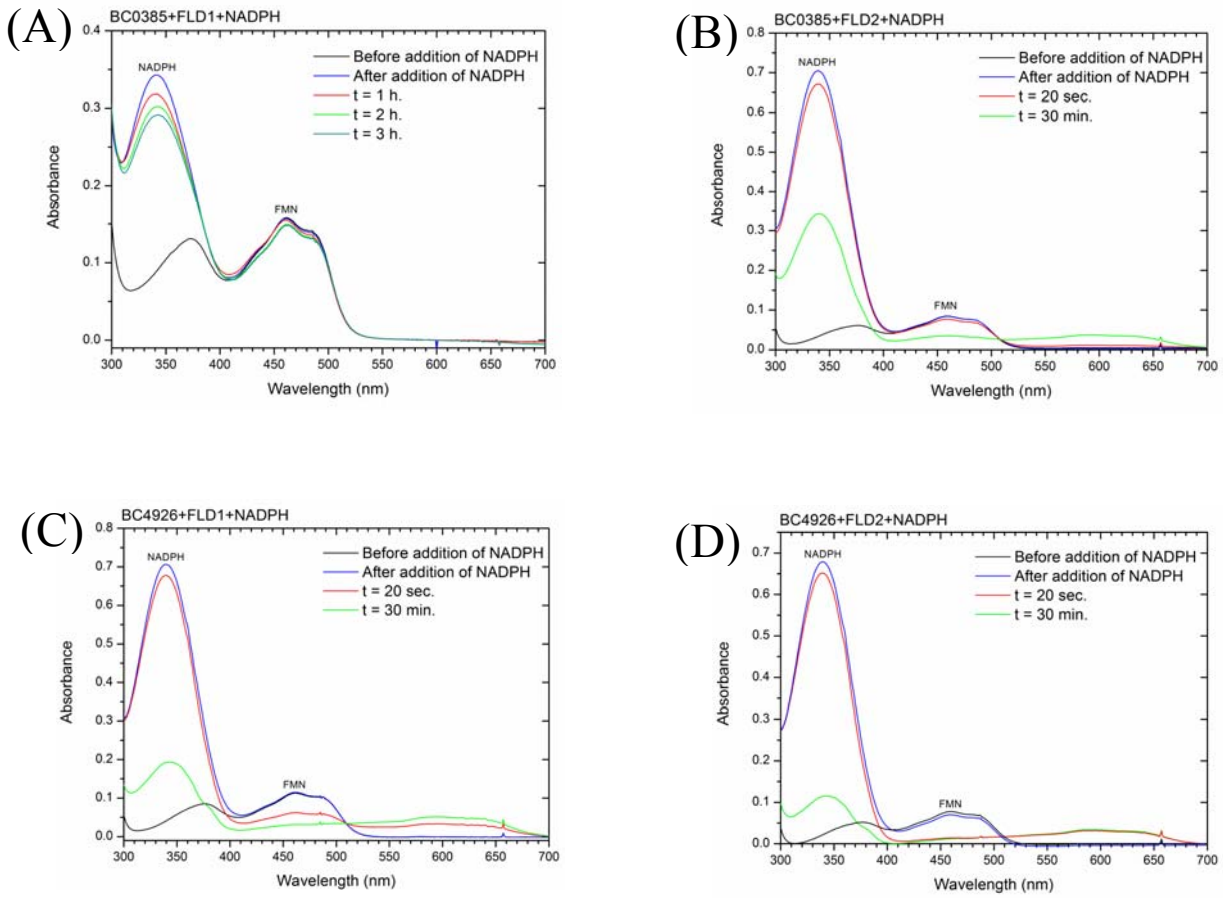

Figure 3.4.4: Absorbance spectra over time from the testing of the ability of the FldRs to reduce Fld BC1376 (FLD1; A and C) and Fld BC3541 (FLD2; B and D), respectively.

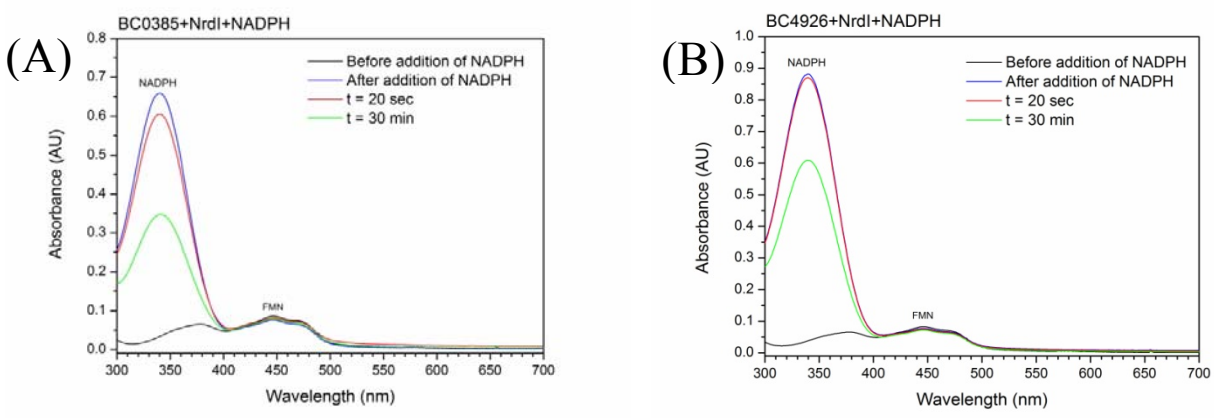

Figure 3.4.4: Absorbance spectra over time from the testing of the ability of FldR BC0385 (A) and FldR BC4926 (B) to reduce NrdI.

4. Concluding discussion and future perspectives

BC0385 was cloned into a pET-22b expressing vector, and *E. coli* BL21 (DE3) cells expressing FldR BC0385 were successfully generated. The protein was over-expressed and purified. In this process, it seemed that the *E. coli* BL21 (DE3) cells produce FldR BC0385 also in the absence of IPTG. This was explained by the fact that in *E. coli* BL21 (DE3) cells, the T7 RNA polymerase is expressed from a promoter which is less sensitive to catabolite repression than the wild type promoter. Because *BC0385* is transcribed by T7 RNA polymerase this could be a reason that expression was observed in the absence of IPTG.

FldR BC4926 was over-expressed and purified as well. During this process, the protein was expressed in two forms in this system; apo-FldR and flavo- FldR. A purification protocol was developed, and a reconstitution experiment indicated that FAD is most likely to be the native flavin cofactor for this protein. An alternative way of confirming the identity of the flavin cofactor could have been to denature the native flavin-containing FldR, purify the flavin cofactor and determine its identity with UV-vis spectroscopy. What remains with respect to the purification protocol, is the establishment of a strategy for reconstitution of flavin-containing FldR. If high amounts of the protein are to be produced, a better reconstitution strategy would be of great interest as the yield of apo-FldR is higher than that of flavo-FldR. The strategy that was tested in this project resulted in a flavo-FldR which precipitated at much lower concentrations than the native flavo-FldR, and which showed to gradually release FAD. The flavin-to-protein ratio seems to be lower than 1 in the sample of native flavo-FldR, which means that apo-FldR is also present in the sample. This could participate in the stabilisation of flavo-FldR at higher concentrations. To test this, different aliquots of FAD could be added to samples of apo-FldR, with subsequent removal of excess FAD and up-concentration. To improve the amount of flavo-FldR obtained, different growth temperatures and lengths of protein expression should also be tested, as this might influence the expression of protein with and without cofactor.

Screening for crystallisation conditions was performed for FldR BC0385 and the three forms of FldR BC4926. Cubic shaped crystals were obtained in the case of FldR BC0385, but they did not show enough diffraction to give a usable dataset for structure solving. However, the crystal system was determined to be monoclinic from initial diffraction experiments. This

indicates that the condition giving these crystals should be tried optimised to give larger crystals in the future work with this protein. In addition, since only two commercial screens were tried out, there is a potentiality for obtaining crystallisation hits with other screens. Because the crystal structure of a protein is highly relevant in understanding its biological function, it is of large interest to do further work in trying to obtain crystals suitable for diffraction experiments.

In the case of FldR BC4926, needle shaped crystals were obtained for both the apo-FldR and the native FldR. The crystals of apo-FldR diffracted very poorly, and diffraction experiments were not tried out for the native FldR crystals. Screening with the native flavo-FldR BC4926 was performed only with three screens. Therefore, future work with this protein should include screening with more commercial screens and subsequent optimisation for eventual hits.

Initial activity measurements suggested that neither of the FldRs is reducing NrdI. On the other hand, NADPH seems to be oxidised in the presence of NrdI and FldR, but not in the absence of FldR. Hence, FldR catalyses either the reduction of O_2 (from system leakage) in these experiments, or it catalyses the reduction of NrdI which then is rapidly re-oxidised by O_2. If the latter is the case, experiments needs to be repeated under more strict anaerobic conditions, where both pH and concentrations of the different components in the reaction are varied. It should also be mentioned that a blind test where NrdI is absent was not performed. This could have indicated if there is a possibility for NrdI to be reduced by FldR, alternatively shown that NADPH is oxidised to the same extent when NrdI is absent, and hence excluded the interpretation of NrdI being reduced by the FldRs.

When tested on Flds from *B. cereus* (BC1376 and BC3541), FldR BC4926 showed to reduce both Flds to their sq form. This might indicate that this FldR has a different redox partner than NrdI *in vivo*. FldR BC0385 did also reduce Fld BC3541 to some extent. This could support the proposal that O_2, rather than NrdI, is reduced in the reactions with FldR and NrdI, because there is a lack of correspondence between the amounts of oxidised NADPH and reduced Fld. This lack indicates that there is another electron acceptor present in the system, namely O_2, which eventually is a more suitable redox partner for FldR BC0385 than is the Fld. Similarly, in the case of NrdI, O_2 is the more suitable redox partner. On the other side, the argument that NrdI might be rapidly oxidised by O_2 *after* being reduced by FldR, can also be used in this

case. However, it might also be that the proper condition for effective reduction of NrdI by FldR remains to be found, and that one or both FldRs actually reduce NrdI *in vivo*.

With DCPIP as the substrate and NADH as the electron donor, initial measurements of kinetic properties revealed that FldR BC0385 has a K_m of 405 µM, and that FldR BC4926 has a K_m of 1.5 µM. Since DCPIP is a two-electron acceptor, this indicates that FldR BC4926 is a 200-fold more effective two-electron donor than FldR BC0385. Interestingly, the case seems to be the opposite with regard to one-electron donation. When NADPH, FldR and the one-electron acceptor Cyt*c* were mixed together, Cyt*c* was more effectively reduced by FldR BC0385 than by the other FldR. This should also be considered in the further work of trying to understand the function of these reductases. In this regard, measuring the ox/sq and sq/hq reduction potentials for both FldRs would give useful insights to their functionality.

With regard to NrdI, it should be searched for other potential reductases, including flavin, iron-sulphur or heme containing proteins in *B. cereus*. However, co-crystallisation with FldR and NrdI would also give insights to potential interactions between the molecules, and should be considered as a future goal.

In summary, this master project presents the very first insights to the behaviour of FldR BC0385 and FldR BC4926. However, further investigations are needed to reveal their function and redox partners in *B. cereus*.

References

1. Abbouni, B., Oehlmann, W., Stolle, P., Pierik, A. J. and Auling, G., 2009, Electron paramagnetic resonance (EPR) spectroscopy of the stable-free radical in the native metallo-cofactor of the manganese-ribonucleotide reductase (Mn-RNR) of Corynebacterium glutamicum. *Free Radical Research,* 43:943-950.
2. Andersson, K. K., 2008. General Short Overview of RNR and Introduction. **In**: K. K. Andersson (ed.) 2008, ***Ribonucleotide Reuctase.*** New York: Nova Science Publishers, Inc. Chapter I.
3. Anjem, A., Varghese, S. and Imlay, J. A., 2009, Manganese import is a key element of the OxyR response to hydrogen peroxide in Escherichia coli. *Molecular Microbiology,* 72:844-858.
4. Armstrong, J., McD., 1964, The molar extinction coefficient of 2,6-dichlorophenolindophenol. *Acta Biochemica et Biophysica,* 86:194-197.
5. Bennett-Lovsey, R. M., Herbert, A. D., Sternberg M. J. E. and Kelley, L. A., 2008, Exploring the extremes of sequence/structure space with ensemble fold recognition in the program Phyre. *Proteins,* 70:611-625.
6. Berg, J. M., Tymoczko, J. L. and Stryer, L., 2007. *Boichemistry.* 6th edition. New York: Sara Tenney.
7. Bergfors, T. M., 1999, *Protein Crystallization: Techniques, Strategies and Tips. A Laboratory Manual.* La Jolla, California: International University Line.
8. Blakley, R. L. and Barker, H. A., 1964, Cobalamide Stimulation of the reduction of Ribotides to Deoxyribotides in Lactobacillus leichmannii. *Biochemical and Biophysical research Communications,* 16:391-397.
9. Blow, D., 2002, *Outline of Crystallography for Biologists.*
10. Boal, A. K., Cotruvo, J. A., Stubbe, J. and Rosenzweig, A. C., 2010, Structural Basis for Activation of Class Ib Ribonucleotide Reductase. *Science,* 329:1526-1530.
11. Boal, A. K., Cotruvo, J. A., Stubbe, J. and Rosenzweig, A. C., 2012, The Dimanganese(II) Site of Bacillus subtilis Class Ib Ribonucleotide Reductase. *Biochemistry,* 51:3861-3871.
12. Bushweller, J. H., Billeter, M., Holmgren, A. and Wutrich K., 1994, The nuclear magnetic resonance solution structure of the mixed disulfide between Escherichia coli glutaredoxin (C14S) and glutathione. *Journal of Molecular Biology,* 235:1585-1597.
13. Cohen, S. S. and Lichtenstein, J., 1960, The Isolation of Deoxyribonucleic Acid from Bacterial Extracts by Precipitation with Streptomycin. *Journal of Biological Chemistry,* 235:PC55-PC56.
14. Cotruvo, J.A. and Stubbe, J., 2008, NrdI, a flavodoxin involved in maintenance of the diferric-tyrosyl radical cofactor in Escherichia coli class Ib ribonucleotide reductases. *Proceedings of the Nathional Academy of Sciences,* 105:14383-14388.
15. Cotruvo, J.A. and Stubbe, J., 2010, An Active Dimanganese(III)-Tyrosyl Radical Cofactor in Escherechia coli Class Ib Ribonucleotide Reductase. *Biochemistry,* 49:1297-1309.

16. Cotruvo, J.A. and Stubbe, J., 2011a, Escherichia coli class Ib ribonucleotide reductase contains a dimanganese(III)-tyrosyl radical cofactor in vivo. *Biochemistry,* 50:1672-1681.
17. Cotruvo, J.A. and Stubbe, J., 2011b, Class I Ribonucleotide Reductases: Metallocofactor Assembly and Repair In Vitro and In Vivo. *Annual review of Biochemistry,* 80:733-767.
18. Crona, M., Torrents, E., Røhr, Å. K., Hofer, A., Furrer, E., Tomter, A. B., Andersson, K. K., Sahlin, M. and Sjöberg, B.-M., 2011, NrdH-Redoxin Protein Mediates High Enzyme Activity in Manganese-reconstituted Ribonucleotide Reductase from Bacillus anthracis. *Journal of Biological Chemistry,* 286:33053-33060.
19. Cox, N., Ogata, H., Stolle, P., Reijerse, E., Auling, G. and Lubitz, W., 2010, A Tyrosyl-Dimanganese Coupled Spin System is the Native Metalloradical Cofactor of the R2F Subunit of the Ribonucleotide Reductase of Corynebacterium ammoniagenes. *Journal of the American Chemical Society,* 132:11197-11213.
20. Draper, R. D. and Ingrahm, L. L., 1968, A potentiometric study of the flavin semiquinone equilibrium. *Archives of Biochemistry and Biophysics,* 125:802-808.
21. Drennan, C. L., Pattridge, K. A., Weber, C. H., Metzger, A. L., Hoover, D. M. and Ludwig, M. L., 1999, Refined structures of oxidized flavodoxin from Anacystis nidulans. *Journal of Molecular Biology*, 294:711-724.
22. Drenth, J., 1999, *Principles of Protein X-ray Crystallography.* 2nd edition. New York: Springer.
23. Dupuy, C., Kaniewski, J., Ohayon, R., Dème, D., Virion, A. and Pommier, J., 2004, Nonenzymatic NADPH-dependent reduction of 2.6-dichorophenol-indophenol. *Analytical Biochemistry,* 191:16-20.
24. Eklund, H., et al., 2001, Structure and function of the radical enzyme Ribonucleotide reductase. *Progress in Biophysics & Molecular Biology,* 77:177-268.
25. Evans, P., 2005, Scaling and Assessment of Data Quality, *Acta Crystallographica Section D: Biological Crystallography*, 62:72-82.
26. Fairman, J. W., Wijerathna, S. R., Ahmad, M. F., Xu, H., Nakano, R., Jha, S., Prendergast, J., Welin, R. M., Flodin, S., Roos, A., Nordlund, P., Li, Z., Walz, T. and Dealwis, C. G., 2011, Structural basis for allosteric regulation of human ribonucleotide reductase by nucleotide-induced oligorimerisation. *Nature Structural and Molecular Biology,* 18:316-322.
27. Fermentas Inc, 2011. *Fast Digestion (with FastDigest® restriction enzymes).* Available at: http://www.fermentas.com/en/support/application-protocols [Last accessed 07.06.12]
28. Fujii, K. and Huennekens, F. M, 1974, Activation of Methionine Synthetase by a Reduced Triphosphopyridine Nucleotide-dependent Flavoprotein System. *Journal of Biological Chemistry,* 249:6745-6753.
29. Gon, S., Faulkner, M. J. and Beckwith, J., 2006, In Vivo Requirement for Glutaredoxins and Thioredoxins in the Reduction of the Ribonucleotide Reductases of Escherichia coli. *Antioxidants and Redox Signaling,* 8:735-742.

30. Hamilton, F. D., 1973, Ribonucleotide Reductase from Euglena gracilis. *Journal of Biological Chemistry,* 14:4428-4434.
31. Hammarsten, E., Reichard, P. and Saluste, E., 1950, Pyrimidine Nucleosides as Precursors of Pyrimidines in Polynucleotides. *Journal of Biological Chemistry,* 183:105-109.
32. Hofer, A., Crona, M., Logan, D. T. and Sjöberg, B.M., 2012, DNA building blocks: keeping control of manufacture. *Critical Reviews in Biochemistry and Molecular Biology,* 47:50-63.
33. Högbom, M., Stenmark, P., Voevodskaya, N., McClarty, G., Gräslund, A. and Nordlund, P., 2004, The radical site in chlamydial ribonucleotide reductase defines a new R2 subclass. *Science,* 305:245-248.
34. Hoover, D. M., Drennan, C. L., Metzger, A. L., Osborne, C., Weber, C. H., Pattridge, K. A. and Ludwig, M. L., 1999, Comparisons of wild-type and mutant flavodoxins from Anacystis nidulans: Structural determinants of the redox potentials. *Journal of Molecular Biology,* 249:725-743.
35. Jiang, W., Yun, D., Saleh, L, Barr, E. W., Xing, G., Hoffart, L. M., Maslak, M-A., Krebs, C. and Bollinger, J. M., 2007, A manganese(IV)/iron(III) Cofactor in Chlamydia trachomatis Ribonucleotide Reductase. *Science,* 316:1188-1191.
36. Johansson, R., Torrents, E., Lundin, D., Sprenger, J., Sahlin, M., Sjöberg, B.-M. and Logan, D. T., 2010, High-resolution crystal structures of the flavoprotein NrdI in oxidized and reduced states – an unusual flavodoxin. *FEBS Letters*, 577:4265-4277.
37. Jordan, A., Aragall, E., Gibert, I. and Barbé, J., 1996, Promoter identification and expression analyses of Salmonella typhimurium and Escherichia coli NrdEF operons encoding one of two class I ribonucleotide reductases present in both bacteria. *Molecular Microbiology,* 19:777-790.
38. Jordan, A., Aslund, F., Pontis, E., Reichard, P. and Holmgren, A., 1997, Characterization of Escherichia coli NrdH. A glutaredoxin-like protein with a thioredoxin-like activity profile. *Journal of Biological Chemistry,* 272:18044-18050.
39. Jordan, A., Pontis, E., Aslund, F., Hellman, U., Gibert, I. and Reichard, P., 1996, The ribonucleotide reductase system of Lactococcus lactis. Characterization of an NrdEF enzyme and a new electron transport protein. *Journal of Biological Chemistry,* 271:8779-8785.
40. Jordan, A., Pontis, E., Atta, M., Krook, M., Gibert, I., Barbé, J. and Reichard, P., 1994, A second class I ribonucleotide reductase in Enterobacteriaceae: Characterization of the Salmonella typhimurium enzyme. *Proceedings of the National Academy of Sciences of the U.S.A.,* 91:12892-12896.
41. Jordan, A. and Reichard, P., 1998, Ribonucleotide Reductases. *Annual review of Biochemistry,* 67:71-98.
42. Kashlan, O. B., Scott, C. P., Lear, J. D. and Cooperman, B. S., 2002, A comprehensive model for the allosteric regulation of mammalian ribonucleotide reductase. Functional consequences of ATP- and dATP-induced oligomerisation of the large subunit. *Biochemistry,* 41:462-474.

43. Kelley, L. A., MacCallum, R. M. and Sternberg, M. J., 2000, Enhanced genome annotation using structural profiles in the program 3D-PSSM. *Journal of Molecular Biology,* 299:499-520.
44. Khangulov, S. V., Barynin, V. V., Voevodskaya, N. V. and Grebenko, A. I., 1990, ESR spectroscopy of the binuclear cluster of manganese ions in the active center of Mn-catalase from Thermus thermophilus. *Biochemical and Biophysical research Communications,* 1020:305-310.
45. Kolberg, M., Strand, K. R., Graff, P. and Andersson, K. K., 2004, Structure, function and mechanism of ribonucleotide reductases. *Acta Biochemica et Biophysica,* 1699:1-34.
46. Krab, K. and Wikström, M., 1979, On the stochiometry and thermodynamics of proton-pumping cytochrome *c* oxidase in mitochondria. *Biochemica et Biophysica Acta,* 584:1-15.
47. Lattman, E. E. and Loll, P. J., 2008, *Protein Crystallography. A consise guide.* Baltimore: The Johns Hopkins University Press.
48. Leadbeater, C., McIver, L., Campopiano, D. J., Webster, S. P., Baxter, R. L., Kelly, S. M., Price, N. C., Lysek, D. A., Noble, M. A., Chapman, S. K. and Munro, A.W., 2000, Probing the NADPH-binding site of Escherichia coli flavodoxin oxidoreductase. *Biochemical Journal,* 352:257-266.
49. Leslie, A.G.W. and Powell, H.R., 2007, Processing Diffraction Data with Mosflm. **In**: Read, R. J. and Sussman, J. L. (eds.) 2007, *Series II Mathematics, Physics and Chemistry Vol. 245*: *Evolving Methods for Macromolecular Crystallography*. Dordrecht: Springer. Chapter 4.
50. Licht, S., Gerfen, G. J., and Stubbe, J., 1996, Thiyl radicals in ribonucleotide reductases. *Science,* 271:477-481.
51. Logan, D. T., Andersson, J. and Sjöberg, B.-M., 1999, A Glycyl Radical Site in the Crystal Structure of a Class III Ribonucleotide Reductase. *Science,* 283:1499-1504.
52. Ludwig, M. L., Pattridge, K. A., Metzger, A. L. and Dixon, M. M., 1997, Control of oxidation-reduction potentials in flavodoxin from Clostridium beijerinckii: The role of conformational changes. *Biochemistry,* 36:1259-1280.
53. Lundin, D., Torrents, E., Poole, A. M. and Sjöberg, B.-M., 2009, RNRdb, a curated database for the universal enzyme family ribonucleotide reductase, reveals a high level of misannotation in sequences deposited to Genbank. *BMC Genomics,* 10:589-596.
54. Madigan, M. T. and Martinko, J. M, 2006. *Brock Biology of Microorganisms.* 11th edition. San Fransisco: Benjamin Cummings.
55. Magnusson, K. E. and Edelbo, L., 1976, Influence of cell concentration, temperature, and press performance on flow characteristics and disintegration in freeze-pressing of Saccharomyces cereciciae with the X-press. *Biotechnology and Bioengineering,* 18:865-883.
56. Mao, S.S., Yu, G. X., Chalfoun, D. and Stubbe, J., 1992, Characterization of C439SR1, a Mutant of Escherichia coli Ribonucleotide Diphosphate Reductase: Evidence That C439 Is a Residue Essential for Nucleotide Reduction and C439SR1 Is a Protein Processing Novel Thioredoxin-like Activity. *Biochemistry,* 31:9752-9759.

57. Massey, V., 2000, The Chemical and Biological Versatility of Riboflavin. *Biochemical Society Transactions,* 28:283-296.
58. McHugh, J.P., Rodriguez-Quiñones, F., Abdul-Tehrani, H., Svistunenko, D. A., Poole, R. K., Cooper, C. E. and Andrews, S. C., 2003, Global iron-dependent gene regulation in Escherichia Coli. A new mechanism for iron homeostasis. *Journal of Biological Chemistry,* 278:29478-29486.
59. Monje-Casas, F., Jurado, J., Prieto-Alamo, M. J., Holmgren, A. and Pueyo, C., 2001, Expression analysis of the NrdHIEF operon from Escherichia coli. Conditions that trigger the transcript level in vivo. *Journal of Biological Chemistry,* 276:18031-18037.
60. New England Biolabs, 2012. *BL21 (DE3) Competent E. coli FAQ.* Available at: http://www.neb.com/nebecomm/products/faqproductc2527.asp#1589. [Last accessed 04.06.12].
61. Nordlund, P. and Reichard, P., 2006, Ribonucleotide Reductases. *Annual review of Biochemistry,* 75:681-706.
62. Novagen, 2003, *pET System Manual* [PDF]. Available at: http://lifeserv.bgu.ac.il/wb/zarivach/media/protocols/Novagen%20pET%20system%20manual.pdf . [Last accessed 09.06.12]
63. Palmer, T., 1991, *Understanding enzymes.* 3rd edition. Chichester: Ellis Horwood Limited.
64. Reichard, P., 1993, From RNA to DNA, why so many ribonucleotides reductases? *Science,* 260:1773-1777.
65. Reichard, P., Baldesten, A. and Rutberg L., 1961, Formation of Deoxycytidine Phosphates from Cytidine Phosphates in Extracts from Escherichia Coli. *Journal of Biological Chemistry,* 236:1150-1157.
66. Roca, I., Torrents, E., Sahlin, M., Gibert, I. and Sjöberg, B.-M., 2008, NrdI Essentiality for Class Ib Ribonucleotide Reduction in Streptococcus pyogenes. *Journal of Bacteriology,* 190:4849-4858.
67. Rofougaran, R., Vodnala, M. and Hofer A., 2006, Enzymatically active mammalian ribonucleotide reductase exists primarily as an α6β2 octamer. *Journal of Biological Chemistry,* 281:27705-27711.
68. Sjöberg, B. M., Reichard, P., Gräslund, A. and Ehrenberg, A., 1977, Nature of the Free Radical in Ribonucleotide Reductase from Escherichia coli. *Journal of Biological Chemistry,* 252:536-541.
69. Stehr, M., Schneider, G., Aslund, F., Holmgren, A. and Lindqvist Y., 2001, Structural basis for the thioredoxin-like activity profile of the gluraredoxin-like NrdH-redoxin from Escherichia coli. *Journal of Biological Chemistry,* 276:35836-35841.
70. Stubbe, J. and van der Donk, W. A., 1998, Protein radicals in enzyme catalysis. *Chemical Reviews,* 98:705-762.
71. Tomter, A. B., Zopparello, G., Andersen, N. H., Hersleth, H.-P., Hammerstad, M, Røhr, Å. K., Sandvik, G. K., Strand, K. R., Nilsson, G. E., Bell, C. B., Barra, A.-L., Blasco, E., Pape, L. L., Solomon, E. I. and Andersson, K. K., 2012, Ribonucleotide reductase class I with different radical generating clusters. *Coordination Chemistry Reviews.* In press. 10.1016/j.ccr.2012.05.021.

72. Torrents, E., Roca, I. and Gibert, I., 2003, Corynebacterium ammoniagenes class Ib ribonucleotide reductase: transcriptional regulation of an atypical genomic organization in the nrd cluster. *Microbiology,* 149:1011-1020.
73. Torrents, E., Sahlin, M., Biglino, D., Gräslund, A. and Sjöberg, B.-M., 2005, Efficient growth inhibition of Bacillus anthracis by knocking out the ribonucleotide reductase tyrosyl radical. *Proceedings of the National Academy of Sciences of the U.S.A.,* 102:17946-17951.
74. Voet, D., and Voet, J. G, 2004. *Biochemistry.* 3rd edition. New York: Wiley.
75. Voevodskaya, N., Lendzian, F., Ehrenberg, A. and Gräslund, A., 2007, High catalytic activity achieved with a mixed manganese-iron site in protein R2 of Chlamydia ribonucleotide reductase. *FEBS Letters*, 581: 3351-3355.
76. Weber, P. C., 1997, Overview of Protein Crystallisation Methods. *Methods in Enzymology,* 276:13-22.
77. Weiner, M. P., Costa, G. L., Schöttlin, W., Cline, J., Mathur, E. and Bauer, J. C., 1994, Site-directed mutagenesis of double-stranded DNA by the polymerase chain reaction. *Gene,* 151:119-123.
78. Willing, A., Follmann, H. and Auling, G., 1988, Ribonucleotide reductase of Brevibacterium ammoniagenes is a manganese enzyme. *European Journal of Biochemistry,* 170:603-611.
79. Worthington Biochemical Corporation, 2012. *Diaphorase Assay.* Available at: http://www.worthington-biochem.com/DIL/assay.html [Last accessed 04.06.12].
80. Zhou, Z. and Swenson, R. P., 1995, Electrostatic effects of surface acidic amino acid residues on the oxidation-reduction potentials of the flavodoxin from Desulfovibrio vulgaris flavodoxin. *Biochemistry,* 34:3183-3192.

Appendix 1: Materials

Table A1.1: Chemicals

Chemical:	**Manufacturer:**
1 kb DNA ladder	Fermentas
6x loding dye solution	Fermentas
10x *Pfu* Buffer with $MgSO_4$	Fermentas
10x FastDigest buffer	Fermentas
Acetic acid (100 %; p.a.)	Merck
Agar	Merck
Agarose	Merck
Ampicillin	CALBIOCHEM
Ammonium acetate	Sigma-Aldrich
Ammonium sulphate (p.a.)	Merck
Bacto Agar	Difco
Bacto Tryptone	Difco
Bacto Yeast Extract	Difco
Bis-Tris	Merck
Bromphenol Blue	Sigma
Buffer R	Fermentas
Calcium chloride	Merck
Coomassie Blue	GE Healthcare
Cytochrome C (bovine heart)	Sigma
Dichlorophenolindophenol (DCPIP)	Worthington Biochemical Corporation
Disodium hydrogen phosphate (p.a.)	Merck
dNTPs (dATP, dCTP, dGTP and dTTP)	Fermentas
DpnI restriction enzyme	Fermentas
E.coli BL21 (DE3)	New England Biolabs
E.coli XL10- Gold ultracompetent	Invitrogen
Ethylenediaminetetraacetic acid (EDTA)	Sigma
Ethanol (Absolutt Prima)	Arcus
Ethidium bromide	GE Healthcare
Fast Digest buffer	Fermentas
Glycerol	Merck
HindIII FastDigest restriction enzyme	Fermentas
Hydrochloric acid	Sigma
Imidazole	Merck
Isopropyl-β-D-Thiogalactopyranoside (IPTG)	Sigma
Low molecular weight standard	GE Healthcare
Magnesium chloride hexahydrate	Merck
Methanol (> 99.5 %; p.a.)	Merck
NdeI FastDigest restriction enzyme	Fermentas
Nicotinamide adenine dinucleotide (NADH)	Sigma-Aldrich
Nicotinamide adenine dinucleotide phosphate (NADPH)	Sigma-Aldrich
Nitrogen (lq)	AGA

pET-22b vector	Novagen
Pfu turbo polymerase	Fermentas
PhastGel Blue R (tablets)	GE Healthcare
Polyethylene glycol 8000	Sigma-Aldrich
Polyethylene glycol 6000	Sigma-Aldrich
Polyethylene glycol 3350	Sigma-Aldrich
Polyethylene glycol monomethyl ether 2000	Sigma-Aldrich
Potassium chloride (p.a.)	Merck
Sodium chloride	Merck
Sodium citrate	Merck
Sodium dihydrogen phosphate	Merck
Sodium hydroxide tablets	Merck
Streptomycin sulphate	Sigma-Aldrich
Tris(hydroxymethyl)aminoethane (> 99.9 %)	Sigma-Aldrich
Zinc acetate	Sigma-Aldrich

Table A1.2: Chromatographic Column Materials

Type of column; material:	**Manufacturer:**
Desalting; Sephadex G-25 Superfine	GE Healthcare
Ion Exchange; Q Sepharose HP	GE Healthcare
Gelfiltration; Cross-linked agarose and dexran	GE Healthcare

Table A1.3: Hardware

Hardware:	**Manufacturer:**
Äkta purifier system	GE Healthcare
HP8452A Spectrophotometer	Hewlett Packard
JA-10 Rotor	Beckman
JA-25.50 Rotor	Beckman
NanoDrop (ND-1000)	NanoDrop Technologies
pH meter (PHM 240)	Radiometer analytical
PhastSystem	Pharmacia

Table A1.4: Chromatographic columns

Column material:	**Manufacturer:**
HiTrap Desalting	GE Healthcare
HiTrap Q HP	GE Healthcare
Superdex 75	GE Healthcare

Table A1.5: Equipment

Equipment:	**Manufacturer:**
Amicon ultra 30K	Millipore
Cryo loops	Hampton Research
Crystal caps and vials	Hampton Research
Crystallization plates (Nextal)	QIAGEN
Cuvettes (quarts)	Helmma
Precision Syringes	Hamilton
Millex-GP 0.22 µm filter	Millipore
PhastGel (10-15 % gradient)	GE Healthcare
PhastGel SDS buffer strips	GE Healthcare

Table A1.6: Kits

Kit:	**Manufacturer:**
NucleoSpin Plasmid	Machery Nagel
Wizard SV Gel and PCR Clean-Up System	Promega

Table A1.7: Commercial crystallization screens

Screen:	**Manufacturer:**
Index	Hampton Research
JSCG+	Quiagen
Natrix	Hampton Research
PEG/Ion	Hampton Research
Wizard I+II	Emerald Biosciences
Midas	Moleclar Dimensions

Appendix 2: PCR mixtures and PCR programs

Table A2.1: PCR of BC0385

Reaction mixture:			**PCR program:**			
1	µL	*Pfu* DNA polymerase (2.5 u/µL)	95	°C	1:00 minute	
2	µL	*B. cereus* genomic DNA	95	°C	0:50 minute	
2	µL	Forward primer (25 µM)	50-68*	°C	0:50 minute	x 30
2	µL	Reverse primer (25 µM)	72	°C	6:00 minutes	
5	µL	dNTP (2 mM)	72	°C	10:00 minutes	
5	µL	10X *Pfu* buffer with $MgSO_4$	4	°C	for ever	
33	µL	mqH_2O				
50	µL	Total volume				

*Gradient for annealing temperatures: 50.0, 51.4, 54.9, 57.6, 63.2, 66.3, 68.0

Table A2.2: PCR for mutagenesis of BC0385

Reaction mixture:			**PCR program:**			
1	µL	*Pfu* DNA polymerase (2.5 u/µL)	95	°C	1:00 minute	
13	µL	Template DNA (75 ng/µL)	95	°C	0:50 minute	
2	µL	Forward primer (25µM)	50-68*	°C	0:50 minute	x 14
2	µL	Reverse primer (25µM)	68	°C	10:00 minutes	
15	µL	dNTP (2mM)	68	°C	10:00 minutes	
5	µL	10X *Pfu* buffer with $MgSO_4$	4	°C	for ever	
12	µL	mqH_2O				
50	µL	Total volume				

*Gradient for annealing temperatures: 50.0, 51.4, 54.9, 68.0

Appendix 3: Restriction- and ligation reaction mixtures

Table A3.1: Double digest mixture for BC0385 and the pET-22b vector

BC0385 reaction mixture			**pET-22b cloning vector mixture**		
4,5	µL	BC0385 (45 ng/µL)	13,5	µL	pET-22b vector (74 ng/µL)
1	µL	NdeI (1 FDU/µL)	1	µL	NdeI (1 FDU/µL)
1	µL	HindIII (1 FDU /µL)	1	µL	HindIII (1 FDU/µL)
3	µL	1x Fast digest buffer	3	µL	1x Fast digest buffer
20,5	µL	mqH_2O	11,5	µL	mqH_2O
30	µL	Total volume	30	µL	Total volume

Table A3.2: Ligation mixture for FldR BC0385 and pET-22b cloning vector

Ligation mixture for NdeI and HindIII digested FldR BC0385 and pET-22b		
6	µL	BC0385 (10 ng/µL)*
7	µL	pET-22b vector (14 ng/µL)*
0,5	µL	T4 ligase
3	µL	Ligation buffer
13,5	µL	mqH2O
30	µL	Total volume

**This gives a 3 times molar excess of BC0385 relative to pET-22b vector*

Appendix 4: Media, buffers, gels and reaction mixtures

Table A4.1: Buffer, gel and reaction mixture for agarose gel electrophoresis

50X TAE buffer:
242 g Tris
100 mL of 0.5 M EDTA
57.1 mL glacial acetic acid
mq H_2O to a final volume of 1000 mL

Agarose gel, 0.8 %:
0.24 g agarose
30 mL 1X TAE buffer

Reaction mixture for DNA purification:

45 µL DNA sample + 6 µL loading buffer
7 µL DNA standard

The DNA was subject to a separation at 95 Volts for 75 minutes in 1X TAE as running buffer.

Table A4.2: Media used for bacterial growth and protein expression

LB-medium:
5 g NaCl
5 g trypton
2.5 g yeast extract
For agar plates: 10 g agar
mq H_2O to a total volume of 500 mL
Adjust to pH 7.5
Sterilise

TB-medium:
12 g trypton
24 g yeast extract
4 mL glycerol (99 %)
mqH_2O to a total volume of 900 mL
Sterilise
100 mL phosphate buffer (add just prior to use)

Phosphate buffer:
2.31 g KH_2PO_4
12.54 g K_2HPO_4
mqH_2O to a total volume of 100 mL
Sterilise

Table A4.3: Solutions and reaction mixtures for SDS-PAGE

Protein cracking solution:

10 mM Tris·HCl (pH 8.0)
1 mM EDTA
0,01 % BFB
2,5 % SDS
5 % mercaptoethanol

0.1 % PhastGel Blue R solution

1 PhastGel Blue R tablet
80 mL mqH2O
120 mL methanol

Stain solution:

1 part 0.2 % PhastGel Blue R solution
1 part 20 % acetic acid

Destain solution:

30 % methanol
10 % acetic acid

Preservation solution:

10 % glycerol
10 % acetoc acid

The protein was subject to a pre-programmed separation script on the PhastGel system, specific for the gradient (10-15 %) in the gel.

Table A4.4: Buffers used in protein purification

Buffer A:
50 mM Tris
5 % glycerol
10 mM EDTA

Adjust to pH 8.1

Buffer B:
50 mM Tris
50 mM NaCl
5 % glycerol

Adjust to pH 8.1

Buffer C:
50 mM Tris
1 M KCl
50 mM NaCl
5 % glycerol

Adjust to pH 8.1

Buffer D:
50 mM Tris
200 mM NaCl
5 % glycerol

Adjust to pH 7.5

The buffers were allways degassed for 15 minutes before used on the chromatography columns.

Table A4.5: Conditions subjected for optimisation for FldR BC4926 apo crystals

	Wizard I+II, H11:	
	Imidazol (pH 8; 0.1 M)	
~15 mg/mL:	$ZnAc_2$ (0.2 M)	
	NaCl (2,5 M)	
	JSCG+, H10:	**JSCG+, H11:**
	Bis-Tris (pH 5.5; 0.1 M)	Bis-Tris (pH 5.5; 0.1 M)
~60 mg/mL:	NH_4Ac (0.2 M)	$MgCl_2$ (0.2 M)
	PEG 3350 (25 % w/v)	PEG 3350 (25 % w/v)

Table A4.6: Conditions subjected for optimisation for FldR BC4926 apo crystals

JSCG+, A7:	**JSCG+, B3:**	**Index, F2:**
CHES (pH 9.5; 0.1 M)	Bicine (pH 8.5; 0.1 M)	Tris (pH 8.5; 0.1 M)
PEG 8000 (20 % w/v)	PEG 6000 (20 % w/v)	Trimethylamine N-oxide (0.2 M)
	(Final pH 9)	PEG MME 2000 (20 % w/v)

Appendix 5: Nucleic acid sequences and primer sequences

A5.1. Mixture for DNA sequencing

Standard mixture details for DNA-sequencing at the ABI-lab at the University of Oslo:

- 8 µL pET-22b with insert (25 ng/µL)
- 2 µL T7 primer or T7 terminator primer (both 5 µM)

A5.2. Nucleic acid sequence of BC0385

ATGAATCGAGAAGAATTGTTTGATGTAACCGTGATAGGCGGAGGACCTGCAGGGCTTTATTCAGCTTTTTATAGT
GGACTCAGAGAAATGAGAACGAAAATAATAGAATTTCACCCACATTTAGGTGGAAAAATACATGTGTATCCGGAA
AAAATGATTTGGGATGTAGGAGGACTATTGCCAGTTACAGGTGATAAGTTAATTGAACAACTTGTACAGCAAGGG
TTAACATTTAAGCCGGAAGTTGTATTAGATACAAAAGTAGAATCGATTATTCGTAATCAAGATGGTACTTTTACA
TTAAAAACAAGTACTGGCGAAGAACACTTTTCAAAAACAGTTATCGTCGCAACAGGAAGTGGTATATTGAAACCG
CAAAAGTTATCTATTGAAGGTGCTGAGCGATTTGAAGTATCGAATTTAAATTATACAGTTAAATCTTTAAAGCGT
TTCAAAGGTAAAACAGTTATTATTTCCGGTGGAGGCAATTCTGCTGTTGATTGGGCAAATGAATTGGAACCAATT
GCGAAAAAAAGTGTATGTAACTTATAGAAAAGAAGAATTATCTGGTCATGAAGCACAAGTAAAACAACTTATGAAC
AGCTCAGCGGAGTGTTTCTTTAATACATCGATTACAAAATTAATTGCCGGTGATAATCATGAAGCGATCGAATAT
GTAGAATTAACAAATCATGAAACAGGTGAGGTTTCTCATTTACCTATTGATGAAGTTATTATTAATCATGGATAT
GAACGCGACATTACATTATTAGAAAATAGTGAGTTAGACGTTGCAATTATAGATAATTATTATATTGCAGGTAAT
GCAAATAGTGAGTCTTCAGTAGATGGATTATATGCTGCTGGAGATATTTTAAAGCACGAAGGGAAACTACACTTA
ATTGCAGGTGCATTCCAAGATGCTGGAAATGCTGTGAATAAAGCAAAACAATTTATCCAACCAGATGCAAGTGAG
TACGGAATGGTTTCTTCTCATAATGAAGTATTTAAGAAGAGAAATCGCGAACTGATTAAGCAGATGATGAAATAA

A5.3. PCR-primers for cloning of BC0385

Forward (NdeI restriction site underlined):
5' – GGAATTCCA|TATGAATCGAGAAGAATTGTTTGATGTAACCG – 3'

Reverse (HindIII restriction site underlined):
5' – AGGA|AGCTTATTTCATCATCTGCTTAATCAGTTCGCG – 3'

A5.4. PCR-primers for point mutation of BC0385

Forward:
5' – GAATTTCACCCACATTTAGGTGG – 3'

Reverse:
5' – CCACCTAAATGTGGGTGAAATTC – 3'